International Journal of Science and Engineering Applications (IJSEA)
Volume 1 Issue 2, 2012, ISSN - 2319-7560 (online)

Study on Advanced High Voltage Capacitor and Its Applications

D.Edison Selvaraj
Department of EEE
Mepco Schlenk Engg., college, Sivakasi
Tamil Nadu India

M.Kiruba Sankar
Department of EEE
Mepco Schlenk Engg., college, Sivakasi
Tamil Nadu India

C.Dinesh Aravind
Department of EEE,
Mepco Schlenk Engg., college, Sivakasi
Tamil Nadu India

Abstract: Owing to meet the advancement in electrical and electronics field modernization is common in all aspects, thus providing latest technologies on capacitors in order to take over the high voltage machineries and transmissions. These capacitors provide good effects on handling high voltage equipments and gadgets. In this paper it shoes the modern capacitor technology that holds high strength dielectrics and can withstand up to great extent in case of high voltages.

Keywords: Impregnation, Bushings, Dielectrics, Fillers, insulation oil.

1. INTRODUCTION

The first capacitor was used in Telephone circuits consists of interleaved sheets of paper and metal foils as dielectric material and paraffin wax was used as impregnant. They can be used only in low voltage circuits. At high voltages, failure occurs due to ionization in the voids formed in wax during cooling. The impregnant paraffin wax was replaced by petroleum jelly. In this case also, troubles occur due to the formation of voids. Hence, petroleum jelly was replaced by Mineral oil. The layers of paper and metal foil were assembled in a small case before impregnation and the case was sealed leaving a filling hole. Chlorinated oil (Penta chloro diphenyl) having pour point of -10 °C and Mineral oil having pour point of -45 °C can also be used as impregnant. A capacitor made with the above grade of chlorinated oil is self compensating with respect to temperature. If the capacitor was de-energized at sub-zero temperature, congealing (becoming semisolid) accompanied by void formation could occur and the capacitor damages.

Recent grades of chlorinated oil

Type	Pour point
Tetrachloro diphenyl	-9 °C
Trichloro diphenyl	-18 °C

At this stage stabilizers were used to improve the life properties, but now-a-days they are restricted to capacitors used on DC applications. In recent days, tests have shown that Wood pulp paper (universally known as Kraft paper) impregnated in chlorinated oil were electrically better. Operating stress in mineral oil and Chlorinated diphenyl was 13.5 V/µm (rms) [130KV/cm]. Nowadays stress up to 20 V/µm (rms) [20KV/cm] is being used.

2. REQUIREMENTS AND PROPERTIES OF THE DIELECTRICS USED IN CAPACITORS

Complete design of a capacitor depends on the dielectric medium used. Any dielectric medium should satisfy electrically, mechanically and chemically. The dielectric should have a best combination of the following properties: Electrical strength tan δ, ε, Cost, Permissible temperature rise the dielectric should have high permittivity, because they permit to get the necessary capacitance with smaller electrode area. In general energy is stored in the dielectric.

The energy is given by,

$W = ½ * CV^2$

The quality of materials necessary for the manufacture of a condenser depends on ε but still more on the working intensity. The working intensity in turn depends on the electric strength of the dielectric, losses in it, etc. The working intensity should be chosen in such a way that it does not exceed the working strength of the dielectric and doesn't cause heating above the permissible temperature. Thus the cost, weight and dimension of any power capacitor depend upon the number and properties of the dielectric.

2.1 Common Dielectric Materials Used

2.1.1 Mica

It was mainly used in high frequency applications. They are rarely used due to their high cost.

2.1.2 Ceramic

This was also ruled out on economic aspects.

2.1.3 Thermoplastic Film

In this case filling the interlayer spaces with oil was difficult.

2.1.4 Paper

It was widely used in the high voltage capacitors. Impregnation of paper increases its dielectric strength and improves its dielectric permittivity. This is due to the fact that the innumerable pores of the paper forming 25 to 30% of the paper volume is replaced by other high quality

insulating material having higher dielectric permittivity. Solid impregnating masses are not used, because during hardening they shrink and pores are not filled with impregnating mass, i.e. air cavity are left as such. Due to this ε of the dielectric material reduces (by 10 to15%) and partial discharges may occur resulting in reduced life of the capacitor.

2.2 Life expectancy of the capacitor

The life of the capacitor will depend upon the over voltage, elevated temperature and the ageing process. For "hot spot" temperature range = 20˚C ton 75˚C Life expectancy is halved for every 5˚C rise in hot spot temperature.

3 GENERAL FEATURES OF CERAMIC CAPACITORS

1. Minimal size, light weight.
2. Use high insulation plastic films and synthetic insulation oil.
3. Easy to install.
4. Little dielectric loss.
5. Keeps temperature stable, prolongs capacitor life.
6. Stable static capacitance.
7. Excellent manufacturing technique and strict quality control means.
8. There exists stable capacitance with little variation due to temperature and high insulation.
9. With plastic film makes its capacitance stable and durable.
10. Adopts non-polluted insulation oil which should be unharmful to human beings, animals and environment.
11. Built in discharge resistor exists, thus safety is assured.

4 A TYPICAL POWER CAPACITOR DESIGN

4.1 Method of Rating Power Capacitor Units

When capacitors were used to improve power factor, the terms of primary corner is the magnetizing current of power load such as induction motors. The product of the magnetizing current and line voltage determines the reactive component of the load and this is usually expressed in lagging volt-ampere. Since the resulting power factor is determined by the extend that the lagging volt-amperes are supplied by capacitors. It is convenient to rate the capacitor in volt-amperes and since the capacitor volt-amperes are reactive, the expression VAR is used. To avoid large numbers the factor of 1000 is used giving the basis of rating, KVAR. A capacitor rated at 1KVAR will draw 1000VA of reactive current.

$KVAR = (E^2 * 2 \Pi f C * 10^{-6}) / 1000$

Where,

E- rms voltage in kV

C- Capacitance in µF

f- Frequency, cycles

The current that a capacitor will draw from the circuit is directly proportional to voltage, capacitance and frequency.

$$I = 2\pi f C * 10^{-6}\ A$$

The capacitive reactance of a capacitor is inversely proportional to frequency.

$$X_c = \frac{1 * 10^{-6}}{2\pi f C}$$

Continuous Working Voltage: Average voltage over in any 24 hours period.

Frequency: When standard capacitors were used on frequency below 60 cycles, the kVAR would be reduced directly with frequency.

Waveform: In the design of capacitors, if the waveforms were not perfect sine wave, operating kVAR was higher due to the effect of harmonics.

Ambient Temperature: All power capacitor units were designed for an ambient temperature of 40oC, but some capacitors such as those rated for 230V and outdoor open-mounted units may be operated ambient temperature of 50oC.

Terminal to case rating: The terminal to case working voltage was not intended to exceed the terminal to terminal voltage.

4.2 Design of Power Capacitor

Consider 15 kVAR, 2400V capacitor unit treated with pentachlorodiphenyl and with a nominal voltage stress of 13.8 $V/\mu m$.

$$VAR = \frac{V^2}{X_c} = V^2 \omega C$$

$$C = \frac{VAR}{\omega V^2} = \frac{VAR}{2\pi f V^2}$$

$$= \frac{15 * 10^3}{2\pi * 50 * 2400^2}$$

$$= 8.29\mu F$$

Adding 7.5% allowance for manufacturing variations this becomes $8.9\mu F$. Higher voltage capacitors are usually made up of series connected groups with the rating of eachgroup not exceeding 1200V.Since the capacitor will consists of two groups in series, each group must have a capacitance $17.82\mu F$.

If the capacitance is made up of 12 sections each $17.82\mu F$ group will consists of 6 sections in parallel and each section must have a capacitance of $\frac{17.82}{6} = 2.97\mu F$.

The area A can be determined from the formula $A = C * T * K$

Where,

A--- Total active area of the dielectric in m2

C--- Capacitance, in μF.

K--- Empirical factor, which includes average assembly pressure, dielectric constant fluid film and paper density. (K=0.025).

Each section consists of seven layers of $12.5\mu m$ paper.

$$T = 7 * 12.5 = 87.5\mu m$$

$$A = C * T * K$$

$$= 2.97 * 87.5 * 0.025$$

$$= 6.497\ m^2$$

Winding Sections: In winding a capacitor section two dielectric and two foils are wound up on the mandrel with one dielectric between the foils and one on the outside of the one foil, so that a foil will always be adjacent in either direction to a dielectric. Therefore the wound length of the section is one-half the total length of dielectrics.

The active width of the dielectric is the area common to both foils. Assume foil width=22.5 cm, Total active area=6.497m2

The length of the winding, $L = \frac{6.497}{2*22.5*10^2} = 14.44m$

To setup for the winding the above section, 14 rolls of paper and two rolls of foil are arranged on the mandrels. One set of seven sheets of paper is first started, then one foil, then a second set of seven sheets of paper and then a second foil. When all the paper and foils are started, the ending must precede unit 14.44m for each foil.

The paper used in winding a capacitor section is wider than foil to provide adequate margins for the prevention of flashover from foil to foil. During the winding operation the winding machine is stopped to permit insertion of tinned copper strips for making contacts with the foils and providing a means of external electrical connection.

4.3 Winding Configurations

There are two types of windings:

1. Flat winding.
2. Cylindrical winding

The capacitor windings are manufactured by windings on a cylindrical mandrel. The windings are initially wrapped on the cylindrical mandrel. They are then removed and pressed flat or retained as such to have a cylindrical shape. The voltage of a single turn capacitor was limited due to the small thickness of the dielectric.

4.4 Design of Different Types of Capacitors

4.4.1 Power Capacitors

They are constructed preferentially with flat windings pressed into cubic packets and tightly enclosed in sheet metal housing. In this way good heat transfer is guaranteed. Also the temperature dependent expansion of the impregnating medium is taken up by the membrane effect of the housing walls. Power capacitors are required for medium voltages. Due to this the leads for the connecting terminals as well as insulation of the windings against the housings are managed well.

4.4.2 Coupling Capacitors

These capacitors as well as the capacitor parts of the capacitive voltage transformers are required for voltages from 110kV upwards and for low power ratings. They are therefore mainly built in an insulated housing type construction. Windings include flat or cylindrical type with internal series connection.

4.4.3 Impulse Capacitors

These windings must have low inductance in the arrangement of windings and at the terminals. For capacitors in impulse voltage generation, their range is greater than 200kV. They also have an insulated housing. Impulse capacitors for low inductance capacitive energy storage must be built with coaxial or strip conductor terminal and current return via housing.

In this type there is short duration over shooting of the inception voltage. The impulse condenser are used as stores of energy in laboratory impulse voltage and current generators.

Operating Field Strength (usually E=(80-100)$V/\mu m$).With long life span--- (30-40)$kV/\mu m$.With limited life span--- up to 100 kV/mm.The sudden discharge of a HV capacitor constitutes high mechanical stressing of the windings and their connections**,** In the above figure the electrostatic force can be calculated using the energy equation,

$$F' = \frac{1}{2}\epsilon_0\, \epsilon_r\, E^2$$

For E=75$V/\mu m$, ϵ_r=4.2----- $F' = 10^5\ N/m^2$=1bar

For a sudden discharge this pressure, withstood earlier in the winding vanishes very abruptly. For an oscillating discharge, pressure oscillations at twice the discharge frequency occur, and the consequence is a strong mechanical alternating stress on the thin metal and insulating foils.

The electromagnetic forces make it essential that the construction of the winding connections should be of high mechanical quality and strength. To keep the magnetic fields by the discharge current 'i' at a minimum, the impulse capacitors must have direct axial current leads at each winding of the metal foils if possible.

Impulse capacitors are subject to operational oscillatory voltages as shown below.

U_0--- charging voltage

k----oscillatory factor

For the stresses so produced the oscillatory factor k is of great significance .In Impulse capacitors for plasma physics measurements, it is usual to aim life time of about N=10000 discharges for k=0.8.

The following graph gives an idea of the relation between operating field strength and the discharge number 'N' expected up to breakdown.

The above graph was based on the oil impregnated paper windings for k=0.8.for k=5 one may expect 4 times the number of discharges to breakdown. Also a decrease in operating field strength by 10% also permits anticipation of 4 times longer life time. By using castor oil further increase in life time is got.

4.4.4 Dc Capacitors

These capacitors are usually charged with a unidirectional voltage and the stored energy is suddenly released through a switch or gap to provide a high current pulse. They have short life (10^6 discharges) and hence possible to operate at high stress (even above inception level).

Advantage of high stress----The size and hence the cost is reduced.

Disadvantage of high stress---- High stress may cause failure of too many windings, resulting in economic loss.

Material Used: *Aluminium loaded paper.*

Advantages of Aluminium loaded paper:

It absorbs the ionic impurities in the impregnant and makes them inert to the electrical stress and high temperature. It absorbs the decomposition products generated due to electrochemical and thermal degradation.

Impregnant: *Cleaned castor oil*

Castor oil has the same dielectric strength as mineral oil.

$\varepsilon = 4.5 - 4.7$

The dielectric constant of the impregnated paper is increased to 5.5 – 6.0. As a result the volume and weight of the capacitor is reduced.

Operating field Strength: With long life span: (25 – 40) kV/mm.With limited life span: up to 100 kV/mm

Smoothing capacitors (mineral impregnated paper): (80 – 100)V/μm

When askarel impregnated paper windings are subjected to direct voltage testing the following data was got.

No. of layers	2	3	4
E_d	100	170	230

Pulse Repetition Rate: Discharge repetition rate of the capacitors of five to six discharges per minute can usually be achieved with only a moderate increase in temperature. Increasing the repetition rate would lead to higher internal temperature. The loss factor also increases with temperature and thermal instability could be reached.

Protection: The capacitors usually discharge into low impedances and hence no fuses re fitted internally but in small banks the fuses are used externally. Discharge resistances are not fitted because of the excessive charging current required.

4.4.5 Ac Capacitors

Material Used: Paper which is mostly impregnated with synthetic polarized liquids of the type of pentachloro diphenyl with permittivity nearly 5 i.e., about 2 times larger than the mineral oil used. By additional special cleaning techniques it is possible to get synthetic polarized liquids with tanδ=(0.003-0.006).The weight gets reduced by (35-40)% of the mineral oil impregnated capacitors.

Operating Field Strength: At 50 cycles, prolonged action of the voltage and absence of over voltages--- (12-14) k V_{rms}/mm. With the possibility of occurrence of internal over voltages--- (8-9) kV_{rms}/mm.

With the possibility of occurrence of internal and external over voltages--- (7-8) kV_{rms}/mm.

At a frequency of 0.1-10 kC prolonged application of voltage and natural cooling--- (3-6) kV_{rms}/mm and with water cooling--- (8-10) kV_{rms}/mm.

Power Capacitors, (I) askarel impregnated paper--- E= (15-20)$V/\mu m$

(ii) askarel impregnated paper/foils--- E=(35-40) $V/\mu m$

Measuring and Coupling capacitors, mineral oil impregnated paper--- E = (10-15)$V/\mu m$

Paper Thickness: (10-25)μm

Windings: Flat, cylindrical. Both series and parallel connection exist. The type of connections varies based on the operating voltage. The following table illustrates the combination for a pack of 12 windings.

Series windings	Parallel	Operating Voltage
1	12	800
2	6	1600
3	4	2400
4	3	3200
6	2	4800
12	1	9600

Fuse Protection: Internal and External fuses. External fuses only

Effect of Internal fuses in:,

(i)Mineral Oil Impregnated Capacitors— Faulty windings are isolated locally and they permit the continued operation of capacitor banks with little inference to operational needs.

(ii)Chlorinated Impregnants—Internal fusing causes carbonization and decomposition into undesirable products and reduces the life of the unit.

Due to the disadvantages of internal fuses. External fuses are mostly preferred.

5. KEY COMPONENTS FOR A COMPLETE DESIGN

There are four key components:

1. Insulation to Case
2. Discharge resistance
3. Bushing
4. Wicking Effect

5.1 Insulation to Case

Layers of paper are wrapped around the capacitor. Thickness of the layer depend on impulse withstand level.

5.2 Discharge resistance

It was required for the safe handling of power frequency capacitors after de-energization. Power loss is less in the discharge resistance when compared to the dielectric loss in capacitor. Increase in temperature is also not high due to this resistance.

5.3 Bushings

They should operate satisfactorily both in dry and wet conditions.

5.4 Wicking Effect

It means to the uniform distribution of the impregnant (oil) in the dielectric. This distribution mainly depends on the material used (i.e., its absorption capability). In order to achieve excelled wicking effect a fibrous surface capacitor tissue paper sandwiched between aluminum foil and polypropylene film. This layer configuration helps in complete drying and void free impregnation. Thus the capacitor is electrically robust and has long life.

6. COMPARISON OF DIFFERENT CAPACITORS

6.1 Comparison between Paper Impregnation with Mineral Oil and Chlorinated Diphenyls

Mineral Oil Impregnation	Chlorinated Diphenyl (askarel)
(i) Used in measuring and coupling capacitors.	(i) Used in power capacitors
(ii) $\epsilon_r = 4.2, \tan\delta < 0.2\%$	(ii) $\epsilon_r = 5.5$. The power density in this case is more than the mineral oil impregnation.
(iii) With persisting overstepping of the inception voltage wax formation and ultimate breakdown at the edges should be expected.	(iii) With askarel on account of the danger of HCl acid formation at the metal edges, special attention should be paid to ensure that the inception voltage is not exceeded even for short duration.

6.2 Compare Single Layer MPP (Metalized Polypropylene) and Two Layer (Film, Paper + Foil) Capacitors

Single layer (MPP)	Two layer – film + paper + foil
(i) quantity of dielectric material used is only 12% to 22% compared to two layer film + paper + foil design.	(i) Quantity of dielectric material used is more than 4.5 to 8 times compared to single layer MPP design
(ii) Output of capacitor will go on reducing with time.	(ii) Output of Capacitor will remain steady over a period of time
(iii) The power factor will go on reducing hence increasing the maximum demand.	(iii) the power factor and maximum demand will remain steady at the corrected value.
(iv) Frequent replacement is necessary to maintain the power factor.	(iv) Working life is long.
(v) Initial cost is much low, but short working life and very costly.	(v) Initial cost is high but with very long dependable working life ultimately proves very economical.

6. CONCLUSION

Thus, the use of intensive techniques for using advanced capacitors for high voltage transmissions and machineries were illustrated above and their special techniques were also shown above. The capacitors are shown are mostly used for high efficient energy transmissions and latest requirements to meet energy needs and high voltage withstanding capacities and the bushing technology shown are of highly efficient and proves of proper efficient transmissions. Using appropriate technology is the smartness on latest trends HV capacitors provide enough needs to make over the faults were others does.

7. ACKNOWLEDGEMENT

The authors express their sincere gratitude to the almighty God and the Lord Jesus Christ for His blessings for this research. The authors also express their sincere thanks to the Department of Mechanical Engineering and Physics, Mepco Schlenk Engineering College, Sivakasi, India and the Division of High Voltage Engineering, College of Engineering, Guindy, Anna University, Chennai, India for the sample preparation and testing of samples.

9. REFERENCES

[1].DR Buehler, Exploratory Research on the Phenomenon of the Movement of **High Voltage Capacitors**. **Journal** of Space Mixing, 2004; Patrick G. Bailey, "Overview Of Antigravity **...** Robert Stirniman, Electrogravitics

[2] Electrostatics & **High Voltage** Links **...** from (ESD **Journal**); **High-voltage** Handbook · Matweb (**capacitor** dielectric search!)

[3] Apparatus **Bushing** Reference **Book**, Gen- eral Electric Co., Bulletin GET- 2525. NEMA Publication No. 107-1964, Reaffirmed by NEMA 1976.

[4] High voltage electrochemical double layer **capacitors** using conductive carbons as additives. M.S. Michael,; S.R.S. Prabaharan.

[5] Design, Analysis and Construction of a *High Voltage Capacitor* **.Author**: Nathan S. Tyler. Approved by: Alexander L. Julian.

[6] High power &performance capacitor by Alexpokryvailo,Costal carp and cliffard scallpati on vol. 38, no.10 IEEE OCT 2010.

[7] Three-Dimensional Heat Transfer Analysis of Pin-Bushing System With Oscillatory Motion: Theory and

Experiment **Author(s):** Jun Wen, Mem. ASME and M. M. Khonsari, Dow Chemical Endowed Chair in Rotating Machinery, Professor, Fellow ASME *Department of Mechanical Engineering, Louisiana State University, 2508 Patrick Taylor Hall, Baton Rouge, LA 70808*

[8] Bushing for power transformer by James .B

[9] Electrical Machines, Second Edition,Smarajit Ghos, Pearson Education India,March 12, 2012.

International Journal of Science and Engineering Applications (IJSEA)
Volume 1 Issue 2, 2012, ISSN - 2319-7560 (online)

Partial discharge characteristics of enamel filled with micro and nano composite of SiO_2 and TiO_2

D. Edison Selvaraj
Asst Professor, Department of EEE,
Mepco Schlenk Engineering college, Sivakasi, India.
Email: edisonsivakasi@gmail.com

Abstract: Partial discharges were in general a consequence of local electrical stress concentrations in the insulation or on the surface of the insulation. A wide group of discharge phenomena such as internal discharges occurring in voids or cavities within solid or liquid dielectrics, surface discharges appearing at the boundary of different insulation materials, corona discharges occurring in gaseous dielectrics in the presence of inhomogeneous fields and continuous impact of discharges in solid dielectrics forming discharge channels were included as partial discharges. It has been observed that the use of nano composites in the matrix of polymeric materials can greatly improve the thermal, mechanical and electrical properties of polymeric nano composites. A nano composite (TiO_2+SiO_2) has been tested as nano filler. The micro particles of TiO_2 and SiO_2 are converted into nano particles with the help of ball mill. Scanning electron microscope (SEM) has been used to augment the particle size of nano composite. These nano composites were mixed with standard (Elmo Luft 1A-FD) enamel with help of ultrasonic vibrator. The partial discharge characteristics of enamel, micro composite (3:1, 1:3, 1:1 of SiO_2 and TiO_2) filled enamel and nano composite (3:1, 1:3, 1:1 of SiO_2 and TiO_2) filled enamel were detailed and analyzed. The partial discharge measurement was carried out in uniform field electrode configurations. The mixing of nano composites of SiO_2 and TiO_2 taken in the proportion of 1:3 with enamel has a significant improvement in the values of partial discharge inception and extinction voltage by 25% and 35% respectively when compared to the partial discharge inception and extinction voltage of the enamel. Similarly, the enamel filled with micro composites of SiO_2 and TiO_2 taken in the proportion of 1:3 has an increase of 19% and 35% in the values of partial discharge inception and extinction voltage respectively when compared to the partial discharge inception and extinction voltage of the enamel.

Keywords: Partial discharge inception voltage, Partial discharge extinction voltage, Ball Mill, SiO_2, TiO_2, Scanning electron microscopy

1. INTRODUCTION

In the last few years, a great deal of attention has been given to the applications of nano dielectrics in the field of electrical insulating materials. It has been reported that the use of nano composites in the matrix of polymeric materials can greatly improve the thermal, mechanical and electrical properties of polymeric nano composites [1].

In the last few years, a great deal of attention has been given to the application of nano dielectrics in the field of electrical materials [2]. Nano dielectrics were a class of materials containing at least one phase at the nanometer scale. It has been reported that the use of nano fillers improves the corona resistance of polyimide films [4]. In addition, the use of nano composites of Silicon Di-Oxide (SiO_2) and Titanium oxide (TiO_2) in low density polyethylene has shown a smaller decrease in the resistivity of the polymeric matrix compared to micro fillers.

A driving force of the nano revolution was a continuous progress in the nano dielectrics towards increasing the level of stability, the reduction in the size and weight of the insulating materials [3]. In this paper, the partial discharge characteristics of enamel, micro composite (3:1, 1:3, 1:1 of SiO_2 and TiO_2) filled enamel and nano composite (3:1, 1:3, 1:1 of SiO_2 and TiO_2) filled enamel were analyzed and detailed.

2. SYNTHESISATION AND CHARACTERIZATION OF NANO PARTICLES

2.1 Ball mill method

There were several methods for creating nano particles, including both attrition and pyrolysis. In attrition, macro or micro scale particles were ground in a ball mill, a planetary ball mill, or other size reducing mechanism.

Ball mill was an efficient tool for converting micro powder into nano powder [1]. There are two ways of grinding: dry process and the wet process. The Silicon dioxide and titanium oxide nano filler was synthesized by this method. The pulverization planetary ball mill was universally applicable for quick dry or wet grinding of inorganic and organic samples. The sample material was crushed and disintegrated in a grinding bowl by grinding balls. The grinding balls and the micro powder in the grinding bowl were acted upon by the centrifugal forces due to the rotation of the grinding bowl about its own axis and due to the rotating supporting disc.

2.2 Characterization of SiO_2 and TiO_2

Nanoparticle characterization was necessary to establish understanding and control of nanoparticle synthesis and applications. Characterization was done by using a variety of different techniques such as transverse and scanning electron microscopy (TEM and SEM), atomic force microscopy (AFM), dynamic light scattering (DLS), x-ray photoelectron spectroscopy (XPS), X-ray diffraction (XRD), Fourier transform infrared spectroscopy (FTIR), ultraviolet-visible spectroscopy and nuclear magnetic resonance (NMR). Hitachi SU1510 was a compact, high performance scanning electron microscope. It was used for analyzing the particle size of SiO_2 and TiO_2 micro and nano particles. High resolution imaging was provided by this electron microscope.

2.3 Curing

The process of converting liquid state enamel into solid state sample is called as curing. The curing method used for enamel was radical initiator curing. In this process DDM (Diamino Diphenyl Methane) was used as curing agent [1]. 80% of enamel and 20% of epoxy resin was taken. DDM was taken in proportion to epoxy resin. For 1g of resin 0.27 g of DDM was added. DDM was melted for 10 minutes for 60-80º C. The enamel, resin and melted DDM were mixed in a beaker. The mixture was poured in the die which is coated by a Teflon sheet. Then the die was heated at 120º C for 2 hours and 130º C for 3 hours in an oven. The die was cooled and the solid sample was taken away from the oven.

3 EXPERIMENTAL RESULTS

3.1 SEM Image Results

The SiO_2 and TiO_2 particles were subjected to scanning electron microscopy to analyze the particle size and structure of the nano particles. The figures 1 to 4 show the SEM analysis of micro range of SiO_2 and TiO_2 before ball mill synthesization method.

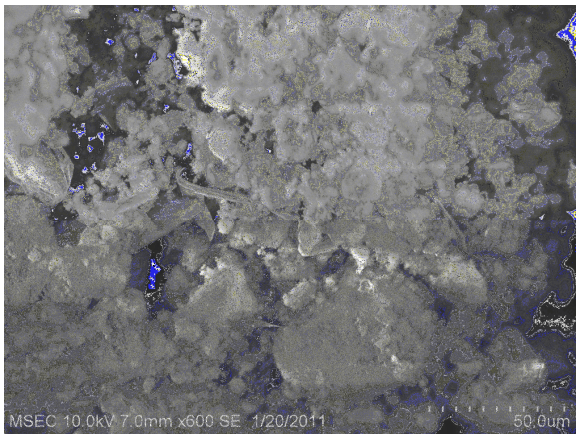

Figure 1 SEM analysis of SiO_2 at 50 μm

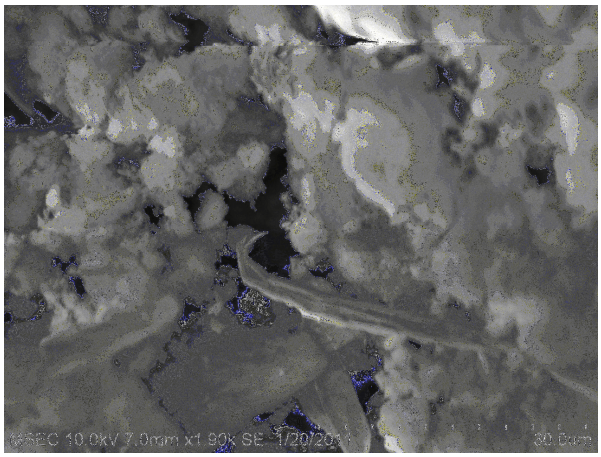

Figure 2 SEM analysis of SiO_2 at 30 μm

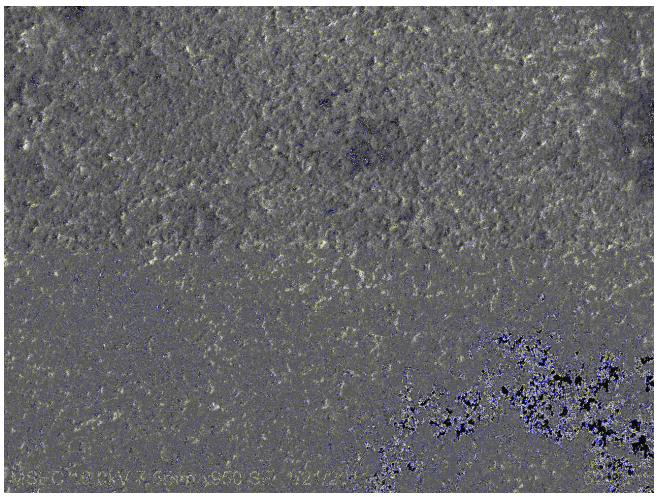

Figure 3 SEM analysis of TiO_2 at 50 μm

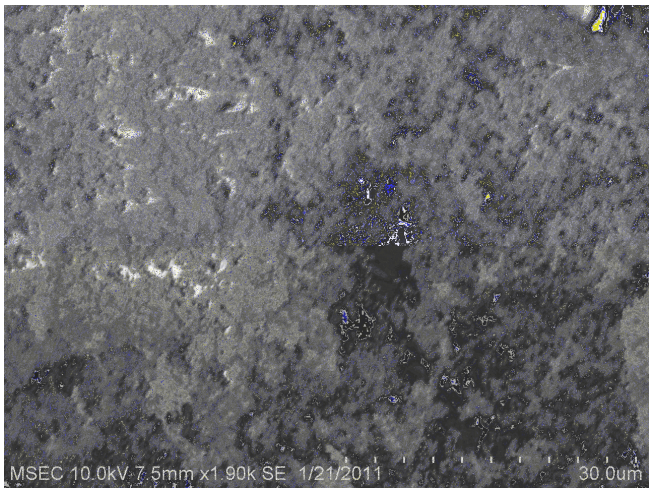

Figure 4 SEM analysis of TiO_2 at 30 μm

The figures 5 to 8 show the SEM analysis of SiO_2 and TiO_2 after ball mill synthesization method.
The micro size particle are converted into nano size with the help of Ball Mill .The SEM results show that the particles were in the form of nano metric range varies. The sizes of the particles were in the range from 40 to 100 nm size.

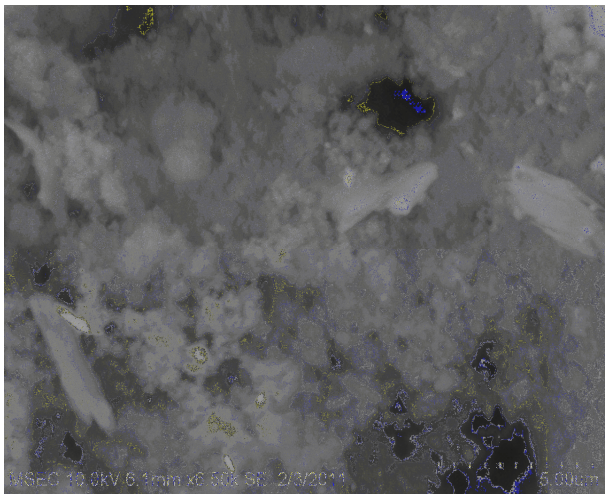

Figure 5 SEM analysis of SiO_2 at 5 μm

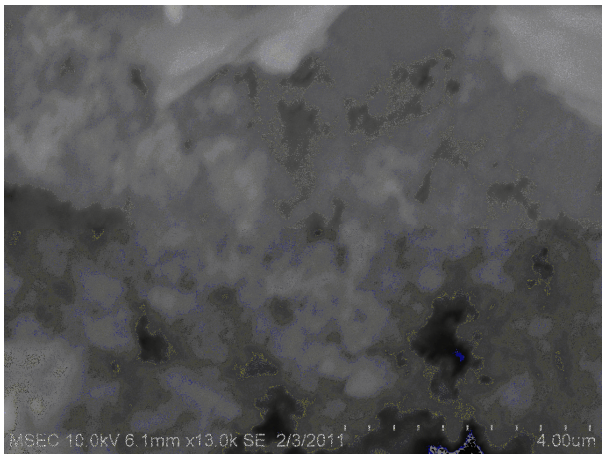

Figure 6 SEM analysis of SiO_2at 4 μm

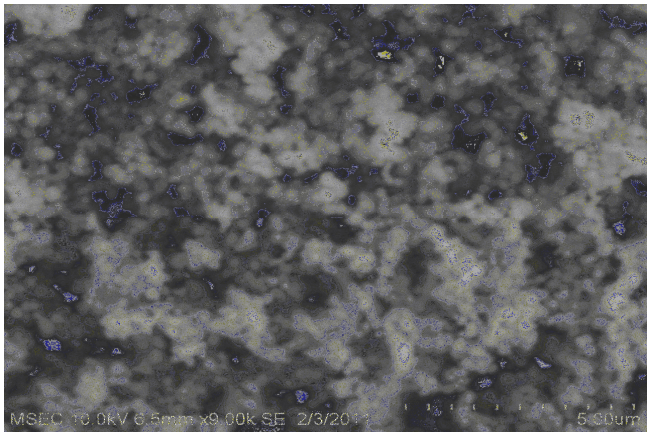

Figure 7 SEM analysis of TiO_2 at 5 μm

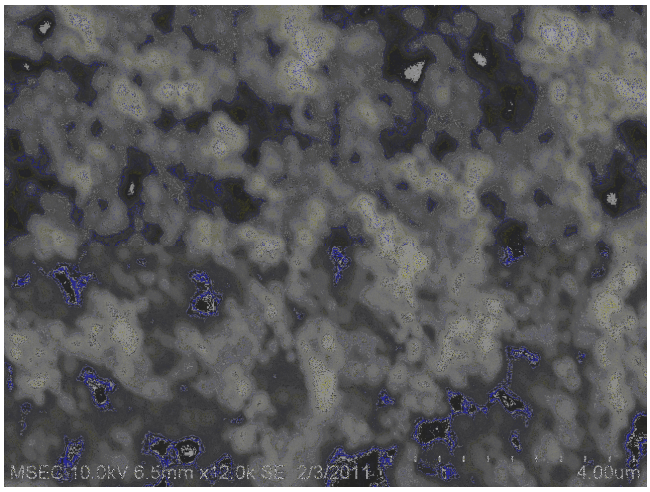

Figure 8 SEM analysis of TiO_2 at 4 μm

3.2 Partial Discharge Measurement

3.2.1 Partial discharge

Partial discharges are in general a consequence of local electrical stress concentrations in the insulation or on the surface of the insulation. Generally such discharges appear as pulses of duration of much less than 1s. The partial discharge includes a wide group of discharge phenomena such as internal discharges occurring in voids or cavities within solid or liquid dielectrics, surface discharges appearing at the boundary of different insulation materials, corona discharges occurring in gaseous dielectrics in the presence of inhomogeneous fields and continuous impact of discharges in solid dielectrics forming discharge channels(treeing).

Every discharge event causes a deterioration of the material by the energy impact of high energy electrons or accelerated ions, causing chemical transformations of many types. The number of discharge events during a closed interval of time is strongly dependent on the kind of voltage applied and will be largest for AC voltages. The actual deterioration is dependent upon the material used. It is still the aim of many investigations to relate partial discharges to the life time of specified materials. The detection and measurement of discharges is based on the exchange of energy taking place during the discharge. These exchanges are manifested as electrical pulse currents, dielectric losses, EMR, sound, increased gas pressure and chemical reactions.

3.2.2 Experimental set up for partial discharge measurement

Partial discharge (PD) current pulses are very sharp pulses having a width of the order of nanoseconds. The IEC 60270 PD detectors are approximated the measured PD pulses as an impulse (less than 500 kHz bandwidth).

Auto Transformer:

Auto transformer takes an input of 220 V, 50Hz, single phase and gives an output varies from 0 to 220V, 50Hz, single phase.

H.V Transformer:

The rating of high voltage transformer is 220/100kV, 50Hz, single phase. By varying the input from 0 to 220V the output varies from 0 to1000kV in proportion. Core made of iron type.

Coupling capacitor:

The coupling capacitor shall be mounted insulated or other measures shall be taken to ensure that ground foil can be connected to the insulated terminal of the measuring impedance AKV-D. Discharge free coupling capacitor is used in this setup. The coupling capacitor should preferably be high. C_c=1000pF.

Measuring Impedance:

AKV-D is the measuring impedance, an inductor in parallel with a capacitor. The measuring impedance unit (Z_m) is located physically close to the high voltage coupling circuit and serves two main purposes:

It attenuates the test voltage present on the high voltage coupling circuit to the safe value for the measurement of the partial discharge signals. It matches the amplifier to the high voltage coupling circuit in insuring a flat frequency response across the full measurement band width. The measuring impedance unit (Z_m) should be configured in such a way as to permit test voltage level monitoring and to observe the phase relationship between the test voltage and the partial discharge pulses; this technique helps to identify the nature of the discharges.

Digital Storage Oscilloscope:

Agilent oscilloscope 54621A is used for the display of the waveforms. The DSO is connected to the DTM at the backend. The oscilloscope displays the phase position of the partial discharge pulses with respect to the AC test voltage. The phase position of the partial discharge pulses with respect to the AC test voltage allows conclusions about the location of the partial discharges in the test object.

The arrangement of electrodes and experimental set up used for partial discharge measurements is shown in the figures 8, 9 and 10.

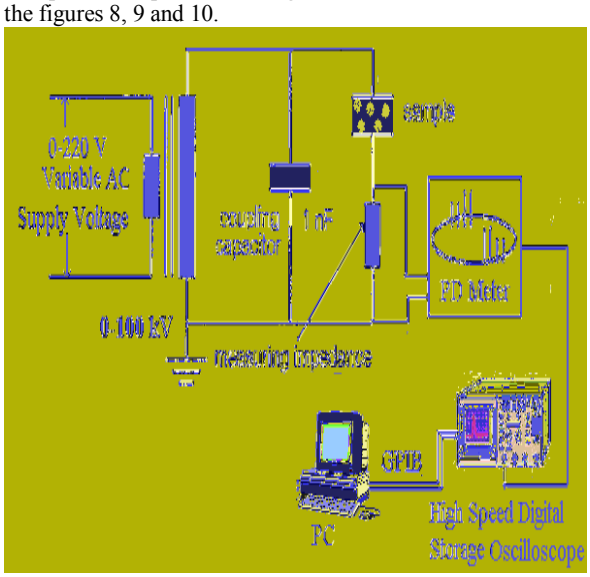

Figure 8 Circuit arrangements for Partial Discharge Measurement

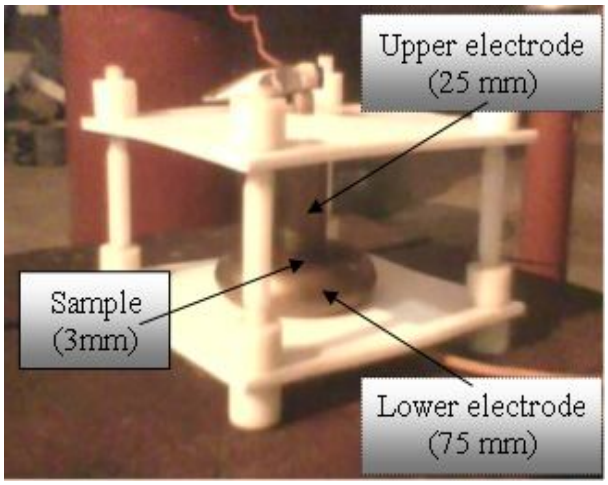

Figure 9 Electrode configuration for PD measurements

Figure 10 Experimental set up for partial discharge measurement for the sample

Plane-plane electrode configuration:

Sample thickness : 3 mm
Diameter of upper electrode : 25mm
Diameter of lower electrode : 75mm
The entire arrangement in an insulating liquid with an appropriate dielectric constant (Ex: Insulating oil).
Allowed pC level:

The allowable pC levels for different conditions are shown in the table 1.

Table 1 Allowable pC level for different conditions

Type of condition	Allowable level
Shielded	Less than 2 pC
Unshielded	7 pC

3.2.3 Experimental Procedure

Before starting the experiment on the test specimen PD meter should be calibrated. The calibrator comprises a pulse generator in series with small capacitor of known value. The generator and the capacitor may be placed in the small box or may be connected together via a properly terminated coaxial cable of sufficient length to permit a calibration from the control room. The pulse generator should either have a known calibrated output level or its output level should be monitored. A suitable output level adjustment in the form of a calibrated potentiometer or a calibrated step attenuator should be provided.

The following three methods specify the test procedure for PD measurements, the first verifies the that test object is free from significant partial discharges up to a specified test voltages; second is used to determine the discharge inception and extinction voltages; and the third is used for measurement of discharge level at a voltage or voltages in range between the inception voltage and the maximum dielectric voltage.

A voltage, well below the specified discharge free voltage, is applied to the test object, gradually increased to the specified voltage, and maintained for the specified time; there after it is decreased and switched off. The object is consider to have the passed the test if the discharges do not exceeded a specified level.

A voltage well below the inception value is applied to the test object and gradually increased until discharge exceeds a specified level. The test voltage at this discharge limit is recorded. The voltage is then increased by 10% and there after reduced to a value at which the discharge ceases or become less than a specified level. The voltage corresponding to this limit is recorded. For some insulation systems, the extinction and inception values may be influenced by the length of the time that the test voltage is maintained above the inception level.

3.2.4 Calibration

The PDG pulse generator is connected in parallel with the test object and normally operated on position “50pC”. The effective PD of the PDG simulates a known partial discharge intensity of the object. With the measuring range selector ‘E’ of the DTM set on the respective position, the display is also set to 50pC with the potentiometer ‘G’ “CORR”. For a defined test arrangement and with identical test objects, the correction factor has to be determined only once and holds good for all the measurements in the setup.

3.2.5 Partial discharge inception and extinction voltage

The partial discharge inception voltage and partial discharge extinction voltage for Plane-Plane electrode configurations were summarized in the following tables 2.

Table 2 The partial discharge inception voltage and partial discharge extinction voltage for Plane-Plane electrode configurations

% of Sample	Inception Voltage KV	pC	Extinction Voltage KV	pC

Pure Enamel	4.34	52	3.1	1.2
1:3 micro	5.15	42	4.2	1.1
3:1 micro	5.02	40	4	1
1:1 micro	4.91	44	3.8	1.3
1:3 nano	5.42	39	4.2	1.2
3:1 nano	5.32	50	4.1	1.1
1:1 nano	5.12	49	3.9	1.1

3.2.6 The measured pulse response of PD inception voltage

The measured pulse responses for PD inception voltage of various samples were shown in figures 9 to 15.

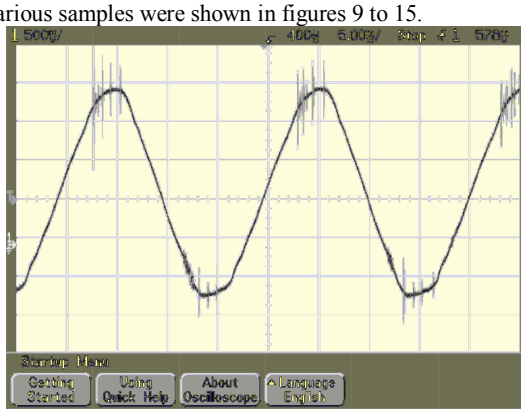

Figure 9 Measured pulse response for PD inception voltage of pure enamel

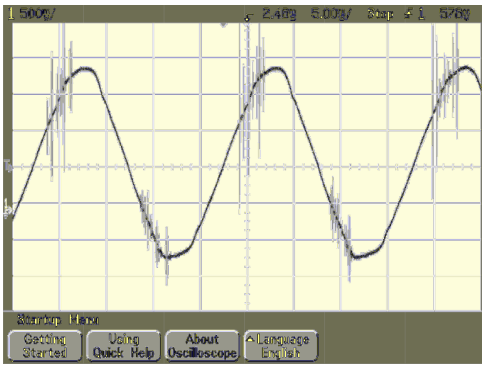

Figure 10 Measured pulse response for PD inception voltage of micro Composites (SiO_2+ TiO_2 -1:3)

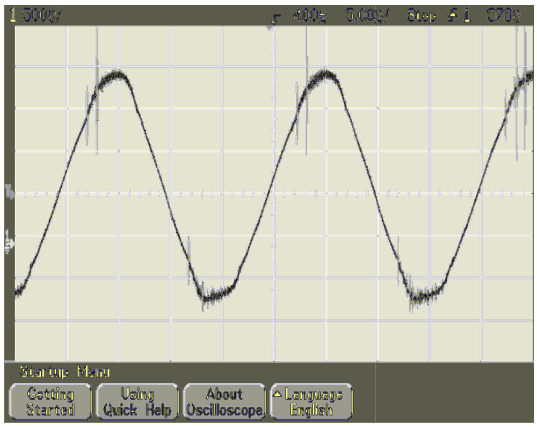

Figure 11 Measured pulse response for PD inception voltage of micro Composites (SiO_2+ TiO_2 -3:1)

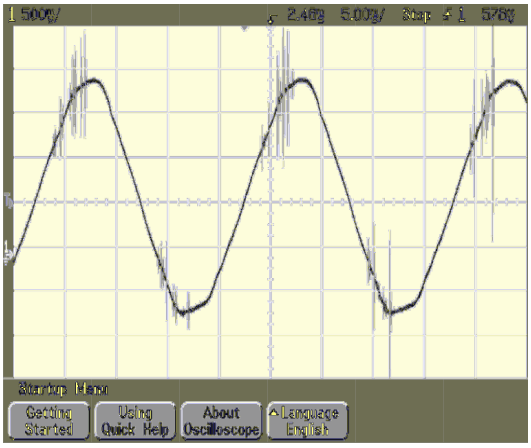

Figure 11 Measured pulse response for PD inception voltage of micro Composites (SiO_2+ TiO_2 -1:1)

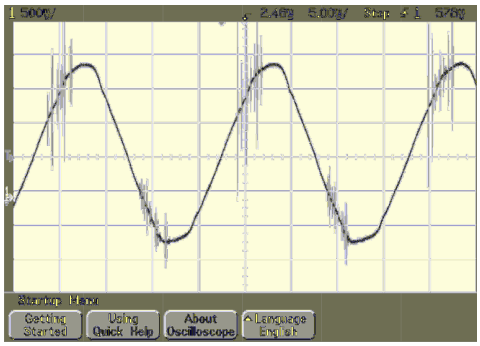

Figure 12 Measured pulse response for PD inception voltage of nano Composites (SiO_2+ TiO_2 -1:3)

Figure 13 Measured pulse response for PD inception voltage of nano Composites (SiO_2+ TiO_2 -3:1)

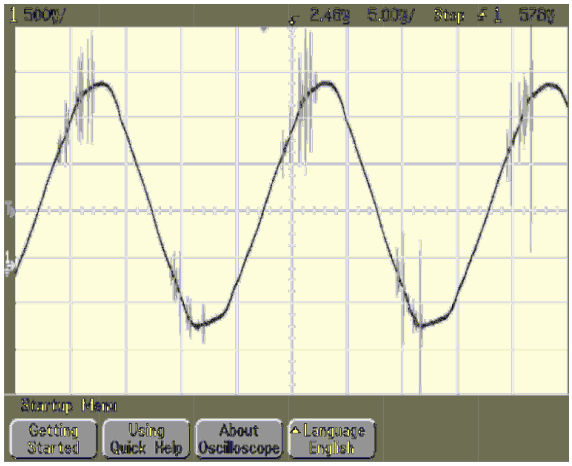

Figure 14 Measured pulse response for PD inception voltage of nano Composites (SiO_2+ TiO_2 -1:1)

4 CONCLUSION

The addition of nano composites of SiO_2 and TiO_2 taken in the proportion of 1:3 as filler with enamel has a significant improvement in the values of partial discharge inception and extinction voltage by 25% and 35% respectively when compared to the partial discharge inception and extinction voltage of the enamel. Similarly, the enamel filled with micro composites of SiO_2 and TiO_2 taken in the proportion of 1:3 has an increase of 19% and 35% in the values of partial discharge inception and extinction voltage respectively when compared to the partial discharge inception and extinction voltage of the enamel.

5 ACKNOWLEDGEMENT

The author expresses his sincere gratitude to the almighty God and the Lord Jesus Christ for His blessings for His research. The authors also express their sincere thanks to the Department of Mechanical Engineering and Physics, Mepco Schlenk Engineering College, Sivakasi, India and the Division of High Voltage Engineering, College of Engineering, Guindy, Anna University, Chennai, India for the sample preparation and testing of samples.

6 REFERENCES

[1] C. Pugazhendhi Sugumaran, M.R.Mohan and K.Udayakumar, “Investigation of Dielectric and Thermal Properties of Nano-filler (ZrO2) Mixed Enamel”, IEEE Transaction on Dielectrics and Electrical Insulation: Vol.17, No.6, 2010.

[2] Hulya Kirkici, Mert Serkan, K.Koppisetty, “Nano-dielectric Materials in Electrical Insulation Application”, IEEE, 2005.

[3] Takahiro Imai, Gen Komiya, Kiyoko Murayama, Tamon Ozaki, “Improving Epoxy-based Insulating Materials with Nano-fillers toward Practical Application”, IEEE 2008.

[4] Guoqin Zhang, Guangning Wu, Laisheng Tong, Enguang, “ Study of Nano TiO_2 Filler in the Corona - resistant Magnetic Wire Insulation Performance of Inverter-fed Motor”, Proceedings of international Symposium on Electrical Insulating Materials, June 5-9, 2005, Kitakyushu, Japan A3-8, 2005.

[5] Edison Selvaraj. D, Pugazhendhi Sugumaran. C and SivaPrakash. A, “Characterization of Electrical and Thermal Properties of Enamel Filled with Carbon Nanotubes”, PEIE 2012, LNEE, pp. 496-502, 2012.

International Journal of Science and Engineering Applications (IJSEA)
Volume 1 Issue 2, 2012, ISSN - 2319-7560 (online)

Characterization of dielectric properties of the enamel filled with carbon nanotubes for the frequency range of 50 Hz - 5 MHz

D. Edison Selvaraj,
Assistant Professor,
Mepco Schlenk Engineering College,
Sivakasi, India.

Abstract:

It has been observed that the addition of nano fillers to the enamel can greatly improve the dielectric properties of the enamel. Carbon nanotubes have been tested as nano filler. Chemical vapour deposition method was used to synthesize carbon nanotubes. Scanning electron microscope has been used to augment the particle size of carbon nanotubes. These carbon nanotubes were mixed with standard (Elmo Luft 1A-FD) enamel with help of ultrasonic vibrator. The basic dielectric properties such as dielectric loss tangent (tanδ), dielectric constant(ε), quality factor, phase angle, dielectric conductivity and dielectric power loss of the enamel filled with carbon nanotubes were analyzed and compared with the properties of the standard enamel. These different dielectric properties were found with the help of the Dielectric Spectroscopy. Dielectric constant, dielectric losses, dielectric conductivity and heat generated under AC fields were analyzed for the frequency range of 50 Hz to 5 MHz. At 50 Hz, the enamel filled with 1 wt% of carbon nanotubes has lower dissipation factor and dielectric losses. At 5 MHz, the enamel filled with 3 wt% of carbon nanotubes has lower dissipation factor and dielectric losses.

Key words – carbon nanotubes, dielectric constant, dielectric losses, dielectric conductivity, quality factor, dielectric loss tangent, dielectric power loss.

1. INTRODUCTION

In the last few years, a great deal of attention has been given to the applications of nano dielectrics in the field of electrical insulating materials. It has been reported that the use of nano composites in the matrix of polymeric materials can greatly improve the thermal, mechanical and electrical properties of polymeric nano composites [4].

In the last few years, a great deal of attention has been given to the application of nano dielectrics in the field of electrical materials. Nano dielectrics were a class of materials containing at least one phase at the nanometer scale. The basic understanding of electrical breakdown of materials and electrical surface flashover phenomena must be investigated before they can be commercially available [1]. The findings of such studies are essential for the development of nano - dielectric materials.

A driving force of the nano revolution was a continuous progress in the nano dielectrics towards increasing the level of stability, the reduction in the size and weight of the insulating materials [5]. The different dielectric properties such as dielectric loss tangent (tanδ), dielectric constant(ε), quality factor, phase angle, dielectric conductivity and dielectric power loss were important for an insulating material [3].

2. EXPERIMENTAL

2.1. Sample Preparation

The nanocomposites were prepared by radical initiator curing method. 80% of enamel and 20% of epoxy resin were taken. Diamino Diphenyl Methane (DDM) was used as curing agent. For 1g of resin, 0.27g of DDM was taken. The DDM was melted at 60° - 80°C for 10 minutes. The enamel, resin and melted DDM were mixed in a beaker. The mixture was poured into the die coated by a Teflon sheet. The die was heated at 120° C for 3 hours. Then, the die was taken away from the oven and it was cooled for 1 hour.

2.2. Synthesis of carbon nanotubes

The synthesis of carbon nanotubes consists of three stages: Preparation of Catalysts for carbon nanotubes, Chemical vapour deposition (CVD) process and Purification of Carbon Nanotubes.

Catalysts with different Mo: Fe: Al_2O_3 molar ratios were prepared by adding calculated amount of Ammonium hexa molybdate tetra hydrate and ferrous sulphate heptahydrate into a suspension of alumina powder in methanol [2]. The different concentrations of catalysts prepared were illustrated in the Table 1.

Table 1 Different catalyst concentrations

S. No	Molar ratio of Mo:Fe:Al_2O_3	Weight of Ammonium hexamolybdate grams	Weight of ferrous sulphate grams	weight of alumina grams	Volume of methanol (ml)
A	0.16:1:16	2.0995	0.8062	9.09	25
B	0.32:1:16	4.199	0.8062	9.09	25
C	0.32:2:16	4.199	1.6124	9.09	25
D	0.48:2:16	6.2985	1.6124	9.09	50

CVD process was done in an experimental set up consisting of a horizontal reaction furnace, Quartz tube, PID controller, Flow meters, Control valves, Gas sources and Thermocouple.

The quartz tube was placed inside the horizontal reaction furnace. A proportional integral differential (PID) controller was provided in the furnace to control the temperature, time and heating rate of the reaction.

Three cylinders of pure Nitrogen (N_2), Acetylene (C_2H_2) and Argon (Ar) were connected to the quartz tube through control valve and flow meter. The rate of carbon and nitrogen entering the reaction tube was shown by the flow meter. Control valves were used to control the flow rate of gases passing through the furnace. Rubber hoses were used to connect the cylinders with flow meter and valves.

After synthesis, the raw products were treated with a solution of KOH (1M) at 80°C in order to remove the alumina support and molybdenum. The resulting material was washed several times with distilled water and then treated with a solution of HCL (1M) in order to remove the remaining iron particles. It was then washed with distilled water.

Then the particle size of the powder was analyzed by using the SEM characterization techniques. From the results, the particle size was found to be tens of nanometer.

2.3. Calculation of relative permittivity, dielectric conductivity and dielectric losses

Dielectric spectroscopy was used to find the loss factor, quality factor and phase angle of the dielectric material. From these factors, dielectric constant, dielectric conductivity, dielectric loss and heat generated under AC fields were found.

Dielectric spectroscopy [LCR HITESTER 3532-50] was also known as Electrochemical Impedance Spectroscopy. The dielectric properties of a medium were measured as a function of frequency. It was based on the interaction of an external field with the electric dipole moment of the sample, often expressed by permittivity.

The set up of dielectric spectroscopy was shown in figure 1.

Figure 1 Dielectric spectroscopy [LCR HITESTER 3532-50]

The real and imaginary part of relative permittivity of the enamel was calculated from the following equations which were used to calculate the dielectric loss [5].

Loss factor $$\tan\delta = \frac{\varepsilon_r''}{\varepsilon_r'} \quad (1)$$

Real part of relative permittivity $$\varepsilon_r' = \left(\frac{t * C_p}{A * \varepsilon_0}\right) \quad (2)$$

Imaginary part of relative permittivity

$$\varepsilon_r'' = \left(\frac{t}{\omega * R_p A * {}_0}\right. \quad (3)$$

Dielectric conductivity $\sigma = \omega * \varepsilon''$ (4)

Dielectric losses $P = 2\pi * f * C * V^2 * \tan\delta$ W (5)

The heat generated under AC field $W_{ac} = E^2 * f * \varepsilon_r * \tan\delta / 1.8 \times 10^{12}$ W/cm^3 (6)

Where
f was the frequency in Hz,
δ was the loss angle of the dielectric material and
E was the applied electric field.
C_p was the equivalent parallel capacitance [F]
R_p was the equivalent parallel Resistance [Ω]
D was the dissipation factor (measured value)
t_m was the average thickness [m]
A was the guarded electrode's surface area [m^2]
D was the guarded electrode's diameter[m]
ε_o was the permittivity of free space =8.854 x 10^{-12} [F/m]
V was the applied voltage [V]

tanδ was the dielectric loss tangent

3. RESULTS

3.1. SEM analysis of Carbon nanotubes

Figure 2 shows the SEM analyzed image results. These results show that particles were in the form of nano metric range. The sizes of the particles were in the range from 50 to 120 nm size.

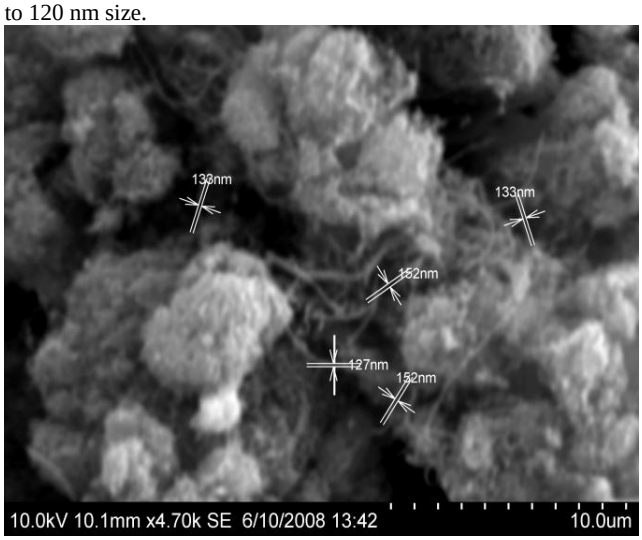

Figure 2 SEM analysis of Carbon nanotubes

3.2. Various dielectric properties of the carbon nanotubes filled enamel for the frequency range (50 Hz to 5 MHz) at 90° C

The different dielectric properties like dissipation factor, quality factor and phase angle were found with the help of the Dielectric Spectroscopy. Dielectric constant, dielectric losses, dielectric conductivity and heat generated under AC fields were analyzed for various frequencies. The loss factor and the quality factor were dependent upon the frequency. The values of various dielectric properties of the carbon nanotubes filled enamel for the frequency range (50 Hz to 5 MHz) at 90° C were listed in the tables 2 to 8.

Table 2 Dissipation factor

Frequency	Enamel	Enamel filled with 1 wt% of carbon nanotubes	Enamel filled with 3 wt% of carbon nanotubes	Enamel filled with 5 wt% of carbon nanotubes
50 Hz	7.865	0.793	0.978	1.083
100 Hz	5.496	0.594	0.59	0.663
1 kHz	1.537	0.274	0.321	0.499
10 kHz	0.508	0.129	0.388	0.229
100 kHz	0.197	0.072	0.137	0.0608
1 MHz	0.121	0.063	0.0877	0.0922
5 MHz	0.0627	0.093	0.0663	0.1282

At 50 Hz, the enamel filled with 1 wt% of carbon nanotubes has lower dissipation factor. At 5 MHz, the enamel filled with 3 wt% of carbon nanotubes has lower dissipation factor.

Table 3 Quality factor

Frequency	Enamel	Enamel filled with 1 wt% of carbon nanotubes	Enamel filled with 3 wt% of carbon nanotubes	Enamel filled with 5 wt% of carbon nanotubes
50 Hz	0.13	1.26	1.02	0.92
100 Hz	0.18	1.68	1.69	1.51
1 kHz	0.65	3.65	3.11	2
10 kHz	1.97	7.72	2.58	4.35
100 kHz	5.06	13.97	7.3	16.43
1 MHz	8.26	15.8	11.39	10.84
5 MHz	15.95	10.65	15.07	7.8

The enamel filled with 1 wt% of carbon nanotubes has higher quality factor at 50 Hz. At 5 MHz, the enamel filled with 3 wt% of carbon nanotubes has higher quality factor.

Table 4 Dielectric constant

Frequency	Enamel	Enamel filled with 1 wt% of carbon nanotubes	Enamel filled with 3 wt% of carbon nanotubes	Enamel filled with 5 wt% of carbon nanotubes
50 Hz	220.35	57.37	104.49	103.37
100 Hz	161.47	51.85	97.14	95.41
1 kHz	76.054	35.66	72.16	58.3
10 kHz	44.51	28.66	38.29	28.36
100 kHz	33.43	25.81	30.03	29.23
1 MHz	28.96	24.5	26.95	28.23
5 MHz	26.39	20.01	23.33	26.16

The value of dielectric constant was high for the enamel at 50 Hz. The lowest value of dielectric constant was observed for the enamel filled with 1 wt% of carbon nanotubes at 5 MHz.

Table 5 Dielectric losses (μW)

Frequency	Enamel	Enamel filled with 1 wt% of carbon nanotubes	Enamel filled with 3 wt% of carbon nanotubes	Enamel filled with 5 wt% of carbon nanotubes
50 Hz	6.17	0.162	0.364	0.4
100 Hz	6.33	0.22	0.41	0.45
1 kHz	8.35	0.697	1.653	2.1
10 kHz	16.11	2.632	10.6	4.9
100 kHz	47.01	13.22	27.53	12.2
1 MHz	250.76	109.79	176.24	172.26
5 MHz	590.63	664.35	551.68	1197.58

The enamel filled with 1 wt% of carbon nanotubes has lowest value of dielectric losses at 50 Hz. At 5 MHz, the enamel filled with 3 wt% of carbon nanotubes has higher value of dielectric losses.

Table 6 Dielectric conductivity (S)

Frequency	Enamel	Enamel filled with 1 wt% of carbon nanotubes	Enamel filled with 3 wt% of carbon nanotubes	Enamel filled with 5 wt% of carbon nanotubes
50 Hz	4.832×10^{-6}	1.567×10^{-12}	9.261×10^{-14}	2.28×10^{-13}
100 Hz	4.95×10^{-9}	4.35×10^{-12}	2.811×10^{-13}	5.80×10^{-3}
1 kHz	6.52×10^{-6}	1.822×10^{-10}	3.63×10^{-11}	1.1×10^{-10}
10 kHz	1.25×10^{-8}	1.338×10^{-8}	8.924×10^{-9}	1.56×10^{-8}
100 kHz	3.68×10^{-8}	1.944×10^{-9}	1.22×10^{-6}	1.17×10^{-6}
1 MHz	1.96×10^{-4}	8.66×10^{-10}	5.86×10^{-4}	9.81×10^{-4}
5 MHz	4.60×10^{-4}	6.2×10^{-11}	57.91×10^{-3}	10.32×10^{-3}

Table 7 Phase angle

Frequency	Enamel	Enamel filled with 1 wt% of carbon nanotubes	Enamel filled with 3 wt% of carbon nanotubes	Enamel filled with 5 wt% of carbon nanotubes
50 Hz	-7.25	-51.55	-45.62	-42.71
100 Hz	-10.31	-59.29	-59.44	-56.46
1 kHz	-33.04	-74.66	-72.18	-63.45
10 kHz	-63.06	-82.62	-68.78	-77.05
100 kHz	-78.82	-85.91	-82.2	-86.52
1 MHz	-83.1	-86.38	-84.98	-84.73
5 MHz	-86.41	-95.36	-93.8	-82.69

Table 8 Heat generated (W/cm^3)

Frequency	Enamel	Enamel filled with 1 wt% of carbon nanotubes	Enamel filled with 3 wt% of carbon nanotubes	Enamel filled with 5 wt% of carbon nanotubes
50 Hz	32.04	0.465	1.56	1.74
100 Hz	32.34	0.632	1.77	2.04
1 kHz	42.61	2.2	7.13	8.9
10 kHz	82	7.64	46.24	25.77
100 kHz	240.3	36.9	127.76	53.38
1 MHz	1277.59	304.01	739.21	773.15
5 MHz	3027.76	1824.05	2448.81	5185.01

The enamel filled with 5 wt% of carbon nanotubes was generating the highest amount of heated at 5 MHz when compared to other samples.

4. CONCLUSION

SEM analysis showed that the prepared carbon particles were appearing in the form of nano metric size. The various dielectric properties were analyzed by dielectric spectroscopy instrument at 90°C for the frequency range of 50 – 5 MHz. These results show that the additions of few weight percentages of carbon nanotubes would improve the dielectric behaviour of the enamel.

5. ACKNOWLEDGEMENT

The author expresses his sincere gratitude to the Almighty God and our Lord Jesus Christ, Division of High Voltage Engineering, Anna University, Chennai, India and the Department of nanotechnology, Mepco Schlenk Engineering College, Sivakasi, India for the sample preparation and testing of samples.

6. REFERENCES

1. Dieter Kind and Hermann Kamer, “High voltage insulation technology” 1985.
2. Jipeng Cheng, et al, (2006) “Carbon nanotube synthesis and parametric study using $CaCO_3$ nanocrystals as catalyst support by CVD” Materials Chemistry and Physics 95, pp 5–11.
3. M S Naidu and V Kamaraju, “High voltage engineering” Solid dielectrics used in practice pp 106 – 122.

4. Nguyen. N. Q, et al, "Investigations on dielectric properties of enameled wires with nanofilled varnish for rotating machines fed by inverters", IEEE 2009.
5. Santanu Singha and Joy Thomas, "Permittivity and tan delta characteristics of epoxy nanocomposites in the frequency range of 1 MHz – 1 GHz", IEEE 2008.
6. Edison Selvaraj. D, Pugazhendhi Sugumaran. C and SivaPrakash. A, "Characterization of Electrical and Thermal Properties of Enamel Filled with Carbon Nanotubes", PEIE 2012, LNEE, pp. 496-502, 2012.

International Journal of Science and Engineering Applications (IJSEA)
Volume 1 Issue 2, 2012, ISSN - 2319-7560 (online)

Voltage Control of Transmission System Using Static Var Compensator

Sandesh Jain
Samrat Ashok Technological Institute
Vidisha, Madhya Pradesh,
India

Shivendra Singh Thakur
Samrat Ashok Technological Institute
Vidisha, Madhya Pradesh,
India

Abstract: This paper will discuss how static Var compensator successfully been applied to control transmission system. The voltage level of the system changes when there is a change in load and the drop in load voltage lead to demand for the reactive power. Static Var Compensator is basically a shunt connected Static Var Generator whose output is controlled by adjust the value of capacitive or inductive current. One of the reasons for installing the Static Var Compensator to improve the voltage profile and increases the system lodability. When system voltage is low it generates the reactive power. When the system voltage is high it absorbs the reactive power. FACTS are technologies that increase flexibility of transmission system, control of power flow and increases transmission capacity of the system. In this paper FACT controller such as Static Var Compensator are used to maintain the voltage within limit. Simulation will be provided by using MATLAB.

Keywords: Voltage Control, FACT, Static Var Compensator, Performance, VAR planning, MATLAB/SIMULINK

1. INTRODUCTION

In presently, power system are large, complex and interconnected system, which consist of thousand of buses and hundreds of generator. In presently electric power system create a need of flexibility, reliability, accuracy and fast dynamic response. Flexible alternating current transmission system is new device that are capable of increase transmission capacity, increase lodability, stability of the transmission system. Static Var Compensator is thyristor based controller that provides rapid voltage control. The situation has occurred increase transient, oscillatory and voltage instability, which are now these problem can be rectified by using Static Var Compensator. Voltage instability is the cause of voltage collapse. The only way to save the system of voltage collapse through control reactive power. Various FACTS device are connected in the transmission line to inject and absorb the reactive power. When it will absorb the reactive power TCR are connected in the transmission line. When it will inject the reactive power TSC are connected in the transmission line.

The Thyristor switched capacitor (TSC)-

It consists of a capacitor, a bidirectional thyristor valve, and a relatively small surge current limiting reactor. This reactor is needed primarily to limit the surge current in the thyristor valve under abnormal operating. When a capacitor is switched into a sinusoidal voltage source, a large current surge flows through the capacitor if the initial voltage across the capacitor is different than the supply voltage at the instant of switching. The current through the capacitor will be finite (corresponding to the steady state value) if the initial capacitor voltage is equal to the supply voltage at the instant of switching. However the rate of change of current will be very high, beyond the rating of the thyristor devices (acting as switches). To limit the it is necessary to insert a reactor in series with the capacitor.

The Thyristor controlled reactor (TCR)-

It consists of a bidirectional thyristor valve, and a current limiting reactor is connected in series. This reactor is needed to limit the surge current. Under high voltage conditions, the SVC will be at its inductive limit and the TCR current may exceed its rated value. To protect the thyristor valves used in TCR, it is necessary to limit the current through it by phase control. To avoid interaction with voltage regulator function, a time delay is introduced (of the order of 100 ms). The over current limiter takes into account the short-term overload capability of the TCR.Series Capacitors have been used in long distance EHV transmission lines for increasing power transfer. The use of series capacitors is generally the most economic solution for enhancing power flow. However, the problem of SSR has deterred system planners from going in a big way for series compensation. While the use of shunt capacitors doesn't have the problem of SSR, they have drawbacks of their effectiveness being dependent largely on their location. Even when a shunt capacitor is located at the midpoint of a long line, it requires much larger rating to achieve the same level of increase in power transfer as a series capacitor.

2. STATIC VAR COMPENSATOR

The Static Var Compensator (SVC), a first generation FACTS controller is taken up for study. It is a variable impedance device where the current through a reactor is controlled using back to back connected thyristor valves. The application of thyristor valve technology to SVC is an of shoot of the developments in HVDC technology. The major difference is that thyristor valves used in SVC are rated for lower voltages as the SVC is connected to an EHV line through a step down transformer or connected to the tertiary winding of a power transformer. The application of SVC was initially for load compensation of fast changing loads such as steel mills and arc furnaces. Here the objective is to provide dynamic power factor improvement and also balance the currents on the

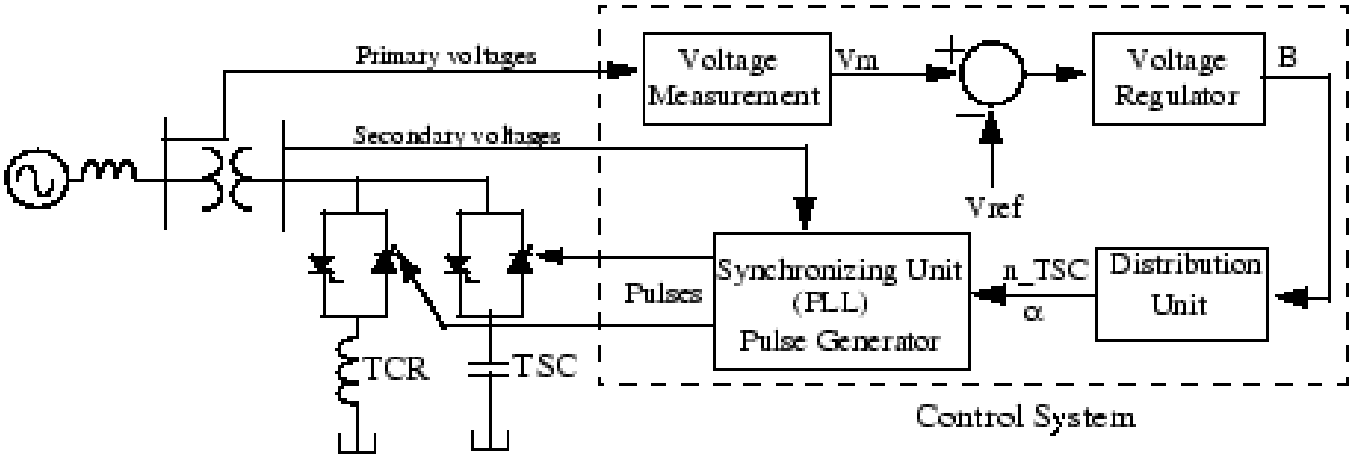

Figure 1.

Compensators commenced in the late seventies. Here the objectives are:

1. Increase power transfer in long lines

2. Improve stability with fast acting voltage regulation

3. Damp low frequency oscillations due to swing (rotor) modes

4. Damp sub synchronous frequency oscillations due to torsional modes

5. Control dynamic over voltages

3. SVC CONTROLLER

SVC Controller incorporating voltage regulator. This shows that both voltage (VSV C) and current (ISV C) signals are obtained from potential and current transformers and then rectified. The AC filter is basically a notch filter to eliminate the signal component of frequency corresponding to the parallel resonance in the system viewed from the SVC bus. The line capacitance (in parallel with SVC capacitance) can result in parallel resonance with the line inductance. The SVC voltage regulator has a tendency to destabilize this resonant mode of oscillation and the notch filter is aimed at overcoming this problem. As a matter of fact, any parallel resonance mode (of frequency below second harmonic) can have adverse interaction with SVC voltage regulator. If series capacitors are used along with SVC, then they can cause parallel resonance with a neighboring shunt reactor. If the second (parallel resonance) mode has a lower frequency (say below 20 Hz), a high pass filter in addition to the Notch filter has been suggested.

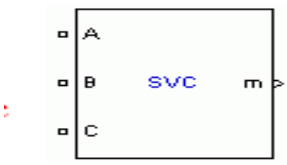

Figure 2

4. SVC V-I CHARACTERISTIC

The SVC can be operated in two different modes: In voltage regulation mode and in var control mode (the SVC Susceptance is kept constant) when the SVC is operated in voltage regulation mode, it implements the following V-I Characteristic. As long as the SVC susceptance B stays within the maximum and minimum susceptance values imposed by the total reactive power of capacitor banks (Bcmax) and reactor banks (Blmax), the voltage is regulated at the reference voltage Vref. However, a voltage droop is normally used (usually between 1% and 4% at maximum reactive power output), and the V-I characteristic has the slope indicated.

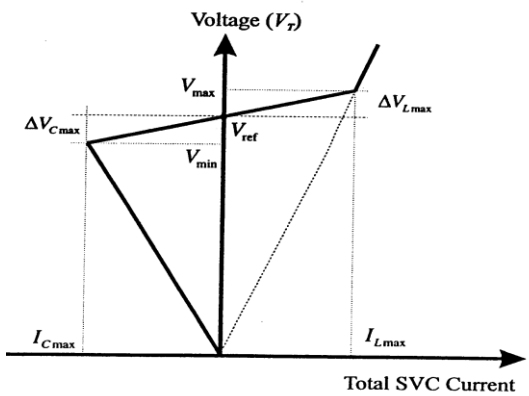

Figure 3

The voltage at which SVC neither absorbs nor generates reactive power is the reference voltage (Vref).In practice this voltage can be adjusted within the typical range of ±10%. The slope of the characteristics reflects a Change in voltage with compensator current and, therefore can be considered as slope reactance, resulting the SVC Response to the voltage variation. Then terminal voltage is given by

VSV C = Vref + XsISV C

ISV C = ¡BSV CVSV C

5. SVC OPERATING WITHIN CONTROL RANGE

The control range of a SVC is defined as, Imin < ISVC < Imax and Vmin< V< Vmax. In this range, the SVC is represented as PV-node at an auxiliary bus with P = 0 and V = Vref. Reactance XSL equivalent to the slope of the V-I characteristics is added between the auxiliary node and node of coupling to the system as shown in Fig. 3. The node at the point of common coupling is a PQ node with P = 0 and Q = 0.

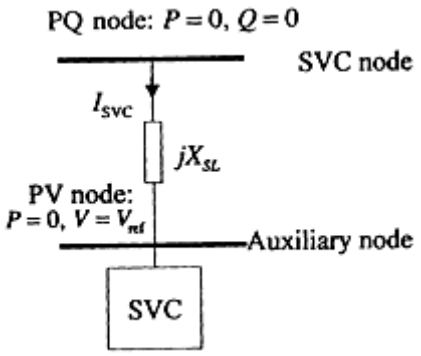

Figure 4

A static var compensator (SVC) is used to regulate voltage on a 33 kV, 3×50 MVA system. When system voltage is low the SVC generates reactive power (SVC capacitive). When system voltage is high it absorbs reactive power (SVC inductive). The SVC is rated+50 Mvar capacitive and 25 Mvar inductive. The Static Var Compensator block is a Phasor model representing the SVC static and dynamic characteristics at the system fundamental frequency. The SVC is set in voltage regulation mode with a reference voltage Vref = 1.0 pu. The voltage droop is 0.03 p.u, 50MVA, so that the voltage varies from 0.97 p.u to 1.015 p.u when the SVC current goes from fully capacitive to fully inductive. By simulating the SVC V-I characteristic curve is obtained. Then, the actual SVC positive-sequence voltage (V1) and susceptance (B1) can be measured with system parameters

Ki = 200
Xn = 0.0667 pu/50 MVA
Xs = 0.03 pu/50 MVA
T=0.0345s

The voltage/current characteristic of the compensator at the 33 kV bus is shown in Fig. 8. The slope of the control range is nominally 3%. This means that a voltage change of -3% produces the rated capacitive reactive power of 50 MVar. For a linear voltage-current characteristic, a voltage changes of +3% produces an inductive reactive power of 50 MVar.

6. CONCLUSION

The proposed technique is applied to a simple power system. It is observed that power increases in the network and control the Bus voltage. Bus voltages of the network also improve. Stability analysis of the system after experiencing fault as well as consequent fault clearance by time domain analysis has also been performed and satisfactory results are obtained.

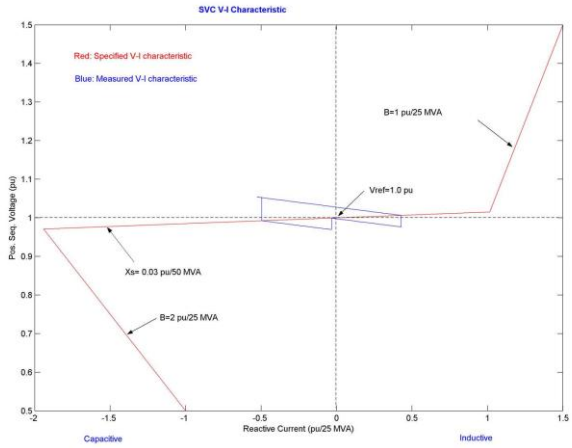

Figure 5

7. REFERENCES

[1] Md. Nazmus Sahadat, Real Power Transfer Capability Enhancement of Transmission Lines Using SVC, IEEE, (2011).

[2] A. H. M. A. Rahim, Voltage Stability Control of a Wind Generation System, IEEE(2010).

[3] Guizhen Tian, Power Quality and Transient Stability Improvement of Wind Farm with Fixed-Speed Induction Generators Using a STATCOM, IEEE **(2010).**

[4] Miller TJ Reactive power Control in Electric Systems. John Willey & Sons (1982).

[5] K. R. Padiyar, FACTS CONTROLLERS IN POWER TRANSMISSION AND DISTRIBUTION, NEW AGE INTERNATIONAL (P) LIMITED, PUBLISHERS(2007).

International Journal of Science and Engineering Applications (IJSEA)
Volume 1 Issue 2, 2012, ISSN - 2319-7560 (online)

Proficient way of Managing Multidimensional Aggregate Data in Unstructured Peer to Peer Networks

Srinivas Raj
LIET, Hyderabad,
India

Murtuza Ahmed Khan
LIET, Hyderabad,
India,

Abstract: the networks which are Peer-To-Peer (P2P) have become very trendy in the last few years. Currently, they are the most common approach to exchange data among large societies of users in the file sharing situation. The capable way of managing storage and retrieval of multidimensional data is achieved by proposed structure which ensures vigorous query development. This structure is based on P2P network, where huge collection of data to be stored. This data is divided into subparts and built up an index on set of each compressed data and this data is to be distributed across p2p networks. This compressed data supports efficient data extraction of information. A duplication method provides suitable coverage of index and metadata by considering network conditions and workload of the queries.

Keywords- multidimensional data, indexing, compression, p2p network, synopsis

1. INTRODUCTION

Currently, they are the most general approach for exchanging data among large societies of users in the file sharing environment. In order to make contributors really independent, they should be forced no restriction on storage and computational resources to be shared, as well as on the consistency of their network connection **[1]**. These necessities make conventional distributed frameworks unsuitable and suggest the implementation of a solution based on an unstructured P2P network, where peers are neither responsible of coordination tasks. The aim is inventing a P2P-based framework supporting the analysis of multidimensional past data. In particular, the efforts are devoted to combine the facilities of P2P networks and data compression to provide a support for the assessment of range queries, possibly trading off effectiveness with accuracy of answers **[2]**. The structure should enable members of an association to cooperate by sharing their resources to host data and perform aggregate queries on them, while preserving their independence. The management of compressed data on unstructured P2P Networks is an interesting issue, but poses several research challenges, which are discussed in the following.

1.1 Compression

A compression technique must be developed which is able to create distributed data supporting the efficient assessment of aggregates, possibly affected by bearable error rates **[3]**. However, in this case, although the rate of disk storage is continuously and quickly decreasing, it may still be hard to find peers for which hosting replicas has a minor cost, while independence is a requirement in the present setting. Using conventional compression techniques, synopsis provides reasonable error rates may have a non-negligible size. Although compressing the data certainly makes replication less resource consuming, replicating the entire synopsis each time would require storage and network resources that could be saved if only some specific portion of the synopsis could be replicated **[4]**. The replication is mandatory in the P2P setting; both to contrast the volatility of peers and to prevent peers from being overloaded are recalled. These drawbacks would be overcome if the compressed synopsis were subdivided into tiny sub synopsis which are independently replicated and distributed on the network when needed. Peers would, therefore, be asked to host replicas of small chunks of data. This way, the independence requirement would not result in a limit on the overall size of the synopsis.

1.2 Indexing

The best way to address this issue is to design an indexing method that supports the efficient location of the sub synopsis involved in the query valuation. In the literature, there are several works proposing distributed indexing methods, where indexes are variants of R-Trees which are partitioned and distributed among the nodes of the network. According to these approaches, nodes of the networks are allocated groups of nodes of the R-tree, and maintain references to hosts which are assigned other nodes of the R-tree. The connection between hosts and R- tree nodes is fixed and the maintenance of the index is centralized. These solutions, as they are, were developed for relatively static situations, and they are not suitable for the dynamic situation addressed by the proposed method, where in order to guarantee peer autonomy, peers cannot be controlled to host a certain portion of the index or to be always connected to the network; and Peers are unstable, so the structure must be capable of promptly reacting to peer disconnections, preventing hanging references in the index **[5]**.

1.3 Replication

A replication scheme capable of maintaining appropriate levels of coverage with respective to the development of user interests and network surroundings must be designed to ensure accessibility and robustness.

The main contributions of this work and its organization may be summed up as follows **[6]**.

- a compression technique for building an indexed aggregate structure over a multidimensional data population, level to be distributed, and accessed across a P2P network;
- a storage model which employs additional data structures to support proficient and robust query answering over compressed data in an unstructured P2P network ; and
- a dynamic replication idea capable of maintaining appropriate levels of coverage with respective to the evolution of the query workload and the network conditions with proposed work.

2. COMPRESSION AND INDEXING DATA

This section consists of three subsections that are partitioning, compression, and indexing.

2.1 Partitioning

The plan of the partitioning step is to divide the data area into non overlapping blocks. These blocks will be compressed separately, yielding distinct sub synopsis. For each of them, a portion of the amount of storage space B chosen to represent the whole synopsis will be invested. The distribution of B among blocks will take into account the following requirements. B must be fairly distributed among blocks and each block must be assigned a “small” portion of B. The task of different amounts of storage space to the blocks for representing their sub synopsis should depend on the differences in homogeneity among the blocks.

Intuitively enough, the more homogeneous the data inside a block, the smaller the amount of information needed to effectively achieve its summarization. The sub synopsis over the blocks is the data that will be hosted by peers and exchanged across the P2P network as shown in the Figure 1. The building of sub Synopsis with “large” size would enforce a significant constraint on the amount of storage space which should be made available by each peer **[7]**. On the converse, defining small-size sub synopsis results in limiting the storage and computational resources required at each peer for storing and querying data, as well as reducing both the download and upload traffic needed for supporting data exchange.

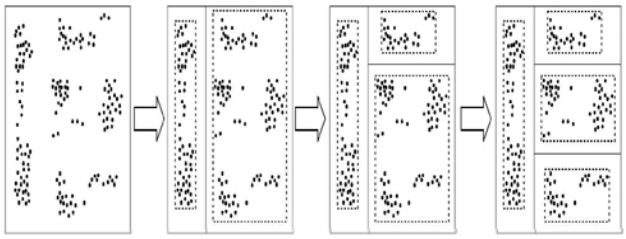

Figure 1: Partitioning a 2D data population

2.2 Compression

Clustering-based Histogram develops a density-based clustering algorithm to construct a set of blocks covering the nonempty portions of the data field **[8]**. For each block its boundaries as well as some aggregate value summarizing its data are stored. In the current implementation, each bucket is connected with the result of evaluating the sum aggregate operator. This way, the summary data suffice to estimate range sum queries.

2.3 Indexing

At this point, an index is built on top of the sub synopsis resulting from the compression step. This index will be developed for locating the data involved in the queries across the network **[9]**. The aggregate R-tree indexing the sub synopsis will be denoted as I as shown in the Figure 2.

.

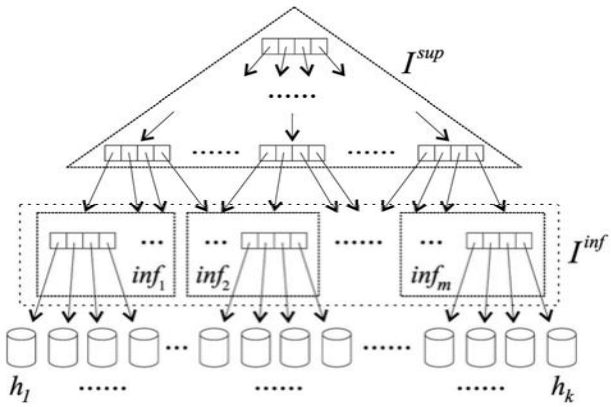

Figure 2: Partitioning the R-Tree

3. PROPOSED METHOD

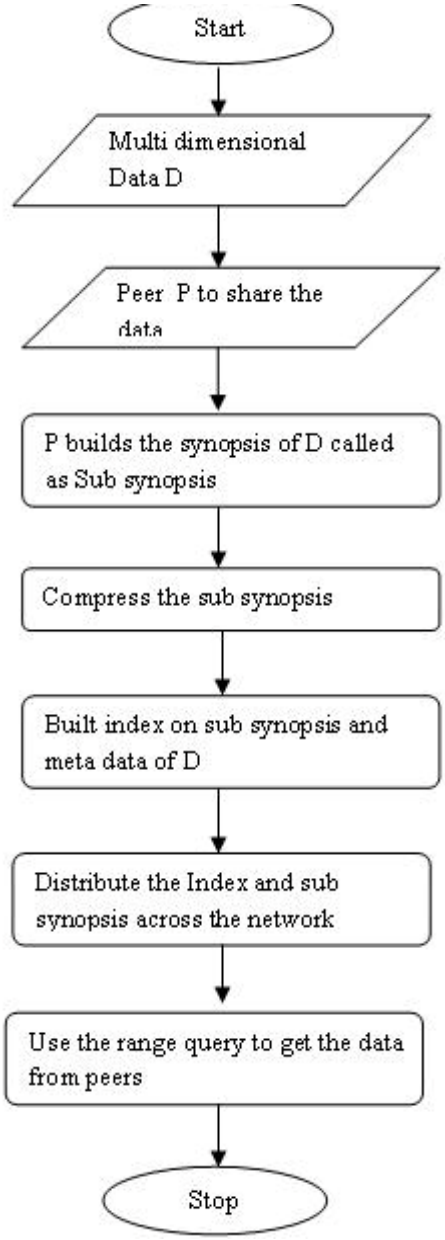

Figure 3: Proposed Method Flow Chart

The aim is devising a P2P-based structure supporting the analysis of multidimensional historical data. Specifically, our efforts will be devoted to combining the facilities of P2P networks and data compression to provide a support for the assessment of range queries, perhaps trading off efficiency with accuracy of answers. The structure should enable members of an society to cooperate by sharing their resources to host data and perform aggregate queries on them, while preserving their independence.

A framework with this uniqueness can be useful in different application environments. For example, consider the case of a worldwide virtual organization with users interested in geographical data, as well as the case of a real institution on an enterprise network. In both cases, even users who are not continuously interested in performing data analysis can make a part of their resources available for supporting analysis tasks needed by others, if their own capability of performing local tasks is preserved **[10]**. This is analogous to the idea on which several popular applications for public resource computing are based in order to make participants really independent, they should be imposed no constraint on storage and computational resources to be shared, as well as on the reliability of their network connection. These requirements make conventional distributed structures unsuitable and suggest the implementation of a solution based on an unstructured P2P network, where peers are neither responsible of coordination tasks, nor imposed to host specific pieces of data.

Nowadays, they are the most widespread approach for exchanging data among large communities of users in the file sharing context specifically, no P2P-based solution has imposed itself as an effective evolution of traditional distributed databases **[11]**. This is quite surprising, as the huge amount of resources provided by P2P networks could efficiently support data management. Our aim is developing a P2P-based structure supporting the analysis of multidimensional historical data. The multidimensional data is stored in peer so that it can be shared in the network, for that built the synopsis. The synopsis is built in three steps

1. Partition 2. Compressing and 3.Indexing.

The aim of the partitioning step is to divide the data domain into non overlapping blocks **[12]**. These blocks will be compressed separately, yielding distinct sub synopsis.

An index is built on top of the sub synopsis resulting from the compression step Index and these sub synopsis are distributed across the network .Queries can be created against the data. The queries can be any explorative queries. One of the first works dealing with the difficulty of supporting range queries in a peer-to-peer network is where data are ordered according to Hilbert curves, and then, distributed among the peers. The compression and indexing processes result in a synopsis organized into sub synopsis, and a fragmented aggregate R-Tree over them. The distribution of the synopsis and the index are performed.

3.1 System Primitives and Data Structures

The existence of two system primitives named search and send. Primitive search (N)—which is used by the structure every time it is required to find sets of peers on the network—returns a set of 'N' IP addresses of randomly chosen peers. In order to choose a peer arbitrarily, it suffices to locate a peer by starting a random walk of length rather than $\log_f N$ (where N is the number of peers in the network and f is the average fan-out) from the peer which invoked search. In fact, a random walk of this length makes the probability of reaching any peer converge to a stationary distribution, which is uniform if the network graph is well connected. In our prototype, the length of the random walk to 1' is set. This allows us to randomly select peers from a network

of up to $4^{1'}$ peers even in the pessimistic case that the network reaches a condition with average fan-out equal to 4. Primitive send(P; o) transmits s-block o from the peer p which invoked the primitives to the peer whose IP addresses are in set P. In our prototype, this primitive properly avoids overloading p when P is large. This is achieved through decentralized dissemination. Instead of sending jPj copies of o, p sends o to a subset of the peers in P which, in turn, keep a copy of o and forward it to different subsets of the remaining peers in P, and so on. We assume that each s- block is uniquely identified throughout the system, and we denote their identifiers as id (I^{sup}), id (inf_i), and id(h_j) **[13]**. Moreover, when needed to avoid confusion, we denote the s-blocks related to a population D as $D.I^{sup}$, $D.inf_i$, and $D.h_j$. Finally, we assume that each s-block carries along metadata about the population it belongs to. These metadata are denoted as Dm and comprise the name of the population, the schema of the data (dimensionality, names, and ranges of dimensions), as well as some keywords which will be exploited to support search operations across the network. The proposed distribution scheme makes use of a set of data structures named as location tables. Each location table will be associated with a copy of an index portion and maintain correspondences between s-blocks and sets of peers. Specifically, the location table associated with I^{sup} will consist of a row for each leaf portion, plus a row for I^{sup} itself. Each row, in turn, will contain addresses of peers where copies of these index portions are hosted. This way, a peer hosting I^{sup} will be able to contact the peers hosting copies of the leaf portions by simply accessing its associated location table. The row for I^{sup} is employed to connect the set of peers that initially host copies of I^{sup} in a clique, i.e., each peer hosting a copy of I^{sup} knows the other peers which are assigned I^{sup} as well. This way, the survivability of populations can be tightly controlled through a mechanism that replaces a peer of the clique as soon as it exits the system. Further details will be provided in the following.

In a location table associated with a copy of a leaf portion inf_i, each row will contain the addresses of the peers hosting copies of a sub synopsis pointed by inf_i . The location tables associated with index portions as table (I^{sup}) and table (inf_i) are denoted. At runtime, the local copies of these tables can be modified by the peers that host them; hence, when needed to avoid confusion, we will denote the tables at a peer p as p.table(I^{sup}) and p.table(inf_i).In addition, along with each sub synopsis and leaf portion, the address of one of the peers that point to it is stored. These reverse pointers allow for more efficient location of the peers involved in the query evaluation Process.

3.2 Disseminating Data and Index

The distribution process is started by a peer p that is willing to publish a data population, and works as follows. First, for each sub synopsis hj (respectively, leaf portion inf_i), p invokes search (C_{min}) to find C_{min} peers which can host a copy of h_j (respectively, inf_i along with table (inf_i)). Then, for each inf_i and sub synopsis h_j referenced by inf_i, location table table (inf_i) is filled with the IP addresses of the peers which will host h_j. Likewise, each h_j is augmented with a reverse pointer to one of the peers which will host inf_i. A similar process is performed to find C_{min} peers which will host I_{sup} along with a location table, and to fill the table as well as the reverse pointers of leaf portions. In meticulous, as explained before, the location table of each peer that will host a copy of I_{sup} is filled with the addresses of the other peers which will host copies of I_{sup}. After all of the location tables have been filled, the copies of s-blocks along with their associated location tables are sent to the appropriate peers. It is worth noting that distributing the copies of the s-blocks randomly across the network well suits the search of data in our unstructured scenario, where search will be performed by randomly navigating across the network. At the same time, the information provided by the location tables allows, once an s-blocks related to a data population D is located, to quickly locate all the other s-blocks that are needed to answer queries over D.

4. RESULTS AND DISCUSSION

Several experiments are performed to review the effectiveness of current approach. Specifically, the accuracy of query estimates and the performance of our copy management strategies in terms of generated network traffic; data reach ability, and query performances are studied.

4.1 Dynamic Replication

The dynamic replication idea aims at both providing the appropriate coverage of s-blocks and balancing the load at the peers. To this intend, besides guaranteeing a minimum coverage for each s-block, replication scheme provides adaptively to the dynamic query workload by creating new replicas of an s-block each time it is queried and by removing less queried data through suitable aging policies. In our structure, location tables encode links among s-blocks spread over the network. Thus, they are kept updated with respective to events causing data unavailability by deleting the addresses of the peers that no longer host these data. The present approach is independent of the way the unavailability of data is identified; in practice, this can be done through periodic pinging. After the deletion of some entries in a location table, the system detects whether the minimum coverage is maintained.

4.2 Query-Based Replication

The two replication strategies, called path based (PBS) and reactive (RS) that aim at increasing the availability of most queried data, also pursuing load balancing when facing large and dynamic query workloads are described.

4.3 Range Queries

The answer of a range query is computed at the requesting peer after receiving the answers of all the (sub) queries submitted to peers hosting data blocks overlapping the query range. The cost of a sub query can be measured from two standpoints, which take into account network-and computation-related costs.

a. Number of hops:

This is at least 1 for a query on I^{sup}, 2 for a sub query on a leaf portion, and 3 for a subquery on a subsynopsis. These values are lower bounds, due to peer volatility, data replacement—which

yield dangling references—and overloading— which triggers the unloading mechanism.

b. Overall wait in queue:

As every (sub) query SQ is enqueued at the peer p' where it will be evaluated, it has to wait for the requests preceding it. The overall wait in queue of SQ is the sum of the enqueuing position of SQ at p^1 and the overall wait in queue of the (sub)query which generated SQ (if any). For instance, if SQ is a sub query on a sub synopsis, its overall wait in queue is the sum of: 1) its enqueuing position at p';
2) the enqueuing position of the sub query SQ' which generated SQ; and 3) the enqueuing position of the query Q which generated sq'.

Thus, an upper bound on the overall time needed to complete the evaluation of a range query Q can be obtained by considering the following quantities:

N_h: the maximum number of hops performed to get the answer of a sub query of Q; and N_q: the maximum overall wait in queue for a subquery of Q.

The diagrams in Figure 4 depict N_h and N_q versus query frequency for different values of Mt(p). Fig. 4'a shows that as query frequency increases, N_h slightly increases. This can be explained as follows: in the case of PBS, a more intensive query workload yields a more frequent data replacements, which increases the likelihood of finding dangling references, and thus, of performing more hops to reach the needed data. In the case of RS, increasing query frequency causes a larger number of peers to be overloaded when they are called to evaluate queries. Thus, the unloading mechanism is triggered, and requests are forwarded to further peers, thus increasing N_h. The increase in query frequency also negatively impacts on N_q (Fig. 4'b). This effect is less evident with PBS, as compared to RS, the higher coverage allows requests to be distributed among a larger number of peers. As expected, for both N_h and N_q, the behavior of RS depends on M_t (p), as RS saturates queues before making replications: thus, waits in queue get longer as $M_t(p)$ increases, whereas the maximum number of hops for answering a sub query decreases since the unloading mechanism, yielding the forwarding of query requests to further peers, becomes less frequent as the capacity of queues increases. The results mentioned above are summarized in the Figure 4. (in the case $M_t(p) = 4$), where the cost of explorative queries (in terms of path length per query) is taken into account as well, thus providing an insight on the overall performance of the query answering process in our framework. To summarize, on the one hand, with PBS, sub queries are more likely to be served first, and the number of hops for getting the "slowest" answer of a sub query is slightly lower. On the other hand, with PBS, explorative queries require longer walks over the network to find the needed data, and the network traffic due to the replications needed to support these performances is much larger than that required by RS, thus making RS a much preferable choice.

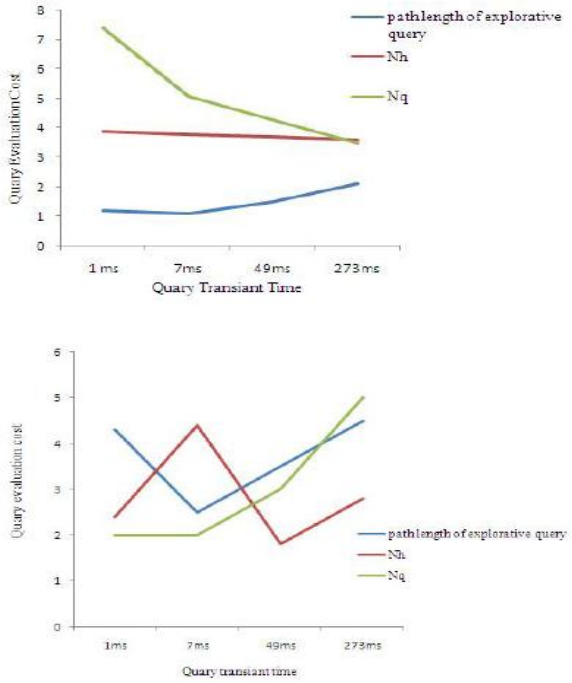

Figure 4: N_h and N_q versus query frequency for different values of Mt (p)

5. CONCLUSIONS & FUTURE WORK

As the importance of peer to peer network is increasing, the data shared in network to be stored and retrieved very efficiently. The proposed framework is to manage the multidimensional data. The data is shared and retrieval in unstructured p2p network. The people, who are interested in sharing their data, make their resources available for all peers in network. So that they can access data by posing range queries .We adopt mechanism for data summarization, data indexing and data distribution and replication by preserving autonomy of peers. The present experiment proves fast and accurate query answers and ensuring the robustness. Future work: adopting these methods to other aggregate operators rather sum. And need to devise suitable compression, indexing techniques and data distributing techniques for better robustness guarantee in the network.

6. ACKNOWLEDGMENTS

The author would like to express their sincere gratitude to the Management, Principal and Vice-Principal of LIET, Hyderabad for their constant encouragement and co-operation.

7. REFERENCES

[1] Giuseppe Massimiliano Mazzeo and Andrea Pugliese Filippo Furfaro, "Managing Multidimensional Historical Aggregate Data in Unstructured P2P Networks," *IEEE TRANSACTIONS ON KNOWLEDGE AND DATA ENGINEERING*, vol. 22, no. 9, pp. 1313-1330, September 2010.

[2] V. Poosala, and S. Ramaswamy S. Acharya, "Selectivity Estimation in Spatial Databases," in *ACM SIGMOD*, 1999.

[3] A. Andrzejak and Z. Xu, "Scalable, Efficient Range Queries for Grid Information Services," in *Proc. Second Int'l Conf. Peer-to-Peer*, 2002.

[4] M. Mihail, and A. Saberi C. Gkantsidis, "Random Walks in Peerto- Peer Networks," in *Proc. 23rd IEEE INFOCOM*, 2004.

[5] S. Chaudhuri and U. Dayal, "An Overview of Data Warehousing and OLAP Technology," *Sigmod Record*, vol. 26, no. 1, pp. 65-74, mar1997.

[6] M. Demirbas and H. Ferhatosmanoglu, "Peer-to-Peer Spatial Queries in Sensor Networks," in *Third Int'l Conf. Peer-to-Peer Computing*, 2003.

[7] http://www.gnutella.com, 2008.

[8] G. Das, D. Gunopulos, and V. Kalogeraki B. Arai, "Approximating Aggregation Queries in Peer-to-Peer Networks," in *Proc. 22nd Int'l Conf. Data Eng*, 2006.

[9] A. Gupta, D. Agrawal, and A. El Abbadi O.D. Sahin, "A Peer-to-Peer Framework for Caching Range Queries," in *Proc. 20th Int'l Conf Data Eng*, 2004.

[10] A. Krishnamurthy, and R.Y. Wang C. Zhang, "Skipindex: Towards a Scalable Peer-to-Peer Index Service for High Dimensional Data," Princeton Univ, Technical Report TR-703-04, 2004.

[11] UCI KDD Archive. http://kdd.ics.uci.edu, 2010.

[12] (2008) http://setiathome.ssl.berkeley.edu.

[13] A. Gupta, D. Agrawal, and A. El Abbadi O.D. Sahin, "A Peer-to-Peer Framework for Caching Range Queries," in *Proc. 20th Int'lConf.*, 2004.

International Journal of Science and Engineering Applications (IJSEA)
Volume 1 Issue 2, 2012, ISSN - 2319-7560 (online)

PERFORMANCE ASSESMENT OF SPATIAL FILTERS IN NOISE REMOVAL BASED ON A DEGRADATION MODEL

S. Sukumaran
Dept. of Computer Science
Erode Arts & Science College, Erode
Tamilnadu. India

M.Shanmugasundaram
Dept. of Computer Science
Erode Arts & Science College, Erode
Tamilnadu. India

Abstract: The most significant feature of images is to reduce Gaussian noise which is commonly found in images and make better image quality. In recent years, technological development has significantly improved analyzing images. Spatial filtering is the method of choice in situations when only additive random noise is present. In this paper, an attempt is made to evaluate the performance of the four linear and non-linear filters used for removing noise from the image. The performance of the noise removal process is analyzed, and the results are compared with the previously reported.

Keywords: spatial filters, Gaussian noise, linear and non linear filter, degradation

1. INTRODUCTION

Filters are widely accepted to remove impulsive and high frequency noise for signal and image processing. The concept of filtering has its roots in the use of the Fourier transform for signal processing in the so-called frequency domain. Spatial filtering term [1] is the filtering operations that are performed directly on the pixels of an image. The process consists simply of moving the filter mask from point to point in an image at each point (x, y) and the response of the filter at that point is calculated using a predefined relationship. Linear and non-linear are two types of filters based on filtering process. In Linear spatial filtering, the result is the sum of products of the mask coefficients with the corresponding pixels directly under the mask.

$$g(x,y) = w(-1,-1)f(x-1,y-1) + w(-1,0)f(x-1,y) + \cdots + w(1,1)f(x+1,y+1) \quad (1)$$

The coefficient w(0,0) coincides with image value f(x,y), indicating that the mask is centered at (x,y) when the computation of sum of products takes place.

For a mask of size m X n, we assume that m=2a+1 and n=2b+1, where a and b are nonnegative integer. Then m and n are odd. In general, linear filtering of an image f of size MxN with a filter mask of size mxn is given by the expression:

$$g(x,y) = \sum_{s=-a}^{a}\sum_{s=-b}^{b} w(s,t)f(x+s,y+t) \quad (2)$$

The process of linear filtering similar to a frequency domain concept called "*convolution*".

$$R = w_1z_1 + w_2z_2 + \cdots + w_{mn}z_{mn} = \sum_{i=1}^{mn} w_i\, z_i \quad (3)$$

$$R = w_1z_1 + w_2z_2 + \cdots + w_9z_9 = \sum_{i=1}^{9} w_i\, z_i \quad (4)$$

Where the w's are mask coefficients, the z's are the value of the image gray levels corresponding to those coefficients. Nonlinear spatial filters are also operated on neighborhoods, and the mechanics of sliding a mask part of an image are the same as was just outlined. The filtering operation is based conditionally on the values of the pixels in the neighborhood under consideration. Smoothing filters [5] are used for blurring and for noise reduction. Blurring is used in preprocessing steps, such as removal of small details from an image prior to object extraction, and bridging of small gaps in lines or curves. Noise reduction can be accomplished by blurring. There are two way of smoothing spatial filters. Smoothing Linear Filters and Order-Statistics Filters. Linear spatial filter is simply the average of the pixels contained in the neighborhood of the filter mask sometimes called "averaging filters". The idea is replacing the value of every pixel in an image by the average of the gray levels in the neighborhood defined by the filter mask. Order-statistics filters are nonlinear spatial filters [4] whose response is based on ordering (ranking) the pixels contained in the image area encompassed by the filter, and then replacing the value of the center pixel with the value determined by the ranking result.

2. IMAGE NOISE MODEL

An image usually contains departures from the ideal signal that would be produced by general model of the signal production process. Such departures are referred to as noise. Noise arises as a result of un-modeled processes available on in the production and capture of the actual signal. It is not part of the ideal signal and may be caused by a wide range of sources, e.g. variations in the detector sensitivity, environmental variations, the discrete nature of radiation, transmission or quantization errors, etc. It is also possible to treat irrelevant scene details as if they are image noise (e.g. surface reflectance textures). The characteristics of noise depend on its source, as does the operator which best reduces its effects. Deliberately corrupting an image with noise allows us to test the resistance of an image processing operator to noise and assess the performance of various noise filters. Noise can generally be grouped into two classes: (i)

independent noise, and (ii) noise which is dependent on the image data. *Image independent noise* can often be described by an additive noise model, where the traced image *f(x,y)* is the sum of the original image *s(x,y)* and the noise *n(x,y)*: i.e. *f(x,y)=s(x,y)+n(x,y).*In several cases, additive noise is equally distributed over the frequency domain (i.e. white noise), while an image contains generally low frequency information. Hence, the noise is dominant for high frequencies and its effects can be reduced using some kind of low-pass filter. This can be done either with a frequency filter or with a spatial filter [8][9]. (Often a spatial filter is preferable, as it is computationally less expensive than a frequency filter.) In the second case of data dependent noise (e.g. arising when monochromatic radiation is scattered from a surface whose roughness is of the order of a wavelength, causing wave interference which results in image speckle), it is possible to model noise with a multiplicative, or non-linear model. These models are mathematically more complicated. Hence, the noise can be assumed as data independent. *Detector Noise* [7] is a kind of noise which occurs in all traced images to a certain extent is detector noise. This kind of noise is due to the discrete nature of radiation, i.e. the fact that each imaging system is recording an image by counting photons. Allowing some assumptions (which are valid for many applications) this noise can be modeled with an independent, additive model, where the noise *n(x,y)* has a zero-mean.

Gaussian distribution described by its standard deviation (σ), or variance. This means that each pixel in the noisy image is the sum of the true pixel value and a random Gaussian distributed noise value [6]. It is difficult to propose a general mathematical model for the effect of the abrasion of the film causing the scratches due to the high number of variables that are involved in the process. However, it is possible to make some physical and geometrical considerations regarding the brightness, thickness, and vertical extent of the line. Line scratches can be characterized as follows: (i) they present a considerable higher or lower luminance than their neighborhoods; (ii) they tend to extend over most of the vertical length of the image frame and are not curved; and (iii) they are quite narrow, with widths no larger than 10 pixels for video images. These features can be used to define a model. The degraded image model considered is

$$a(x,y) = I(x,y)\big(1 - b(x,y)\big) + b(x,y)\,c(x,y) \quad (5)$$

where *I(x,y)* is the pixel intensity of the uncorrupted signal, *b(x,y)* is a detection variable which is set to 1 whenever pixels are corrupted and 0 otherwise, *c(x,y)* is the observed intensity in the corrupted region. This model is applied in this work to images degraded by impulses, strip lines, drop lines, band missing, and blotches.

If *b(x,y)=0* then

$$a(x,y) = I(x,y)(1-0) + 0.c(x,y) = I(x,y) \quad (6)$$

where *I(x,y)* is the original pixel value (uncorrupted pixel). If *b(x,y)=0* then

$$a(x,y) = I(x,y)(1-1) + 1.c(x,y) = c(x,y) \quad (7)$$

where *c(x,y)* is the original pixel value (uncorrupted pixel). Assume that each pixel at *(x,y)* is corrupted by an impulse with probability p independent of whether other pixels are corrupted or not. For images corrupted by a negative or positive impulse, the impulse corrupted pixel *e(x,y)* takes on the minimum pixel value smin with probability *p*, or *s(x,y)* the maximum pixel value smax with probability *1-p*. The image corrupted by blotches or scratches (impulsive) can be now modeled as

$c(x,y) = e(x,y)$ with *p s(x,y)* with *1-p* *(8)*

This, in fact, is the model that describes impulse noise in the literature. However, the existing impulse filtering algorithms do not effectively remove clotches and scratches. In Section 3, an adaptive length median/mean filter algorithm is developed that removes blotches, scratches effectively along with impulse noise.

3. FILTERING METHODS

In this section, we provide the definitions of some linear and non-linear image filters. The expression given below can be used to define image processing function in the spatial domain.

$$f(x,y) = \gamma\big(g(s,t)\big) \quad (9)$$

where γ is the transformation function, g(s,t) is the pixel value of the point p(x, y) of input image, and f(x,y) is the pixel value of the corresponding point of the processed image.

3.1 Arithmetic mean filter

S_{xy} represent the set of coordinates in mask m X n, centered at a point (x,y). This filter takes input as a corrupted image to calculate it's average value in the area defined by $S_{xy.}$ This filter calculate arithmetic mean of restored image f at point (x,y) using the pixel in the area defined by $S_{xy.}$

$$f(x,y) = \frac{1}{mn}\sum_{(s,t)\in S_{xy}} g(s,t) \quad (10)$$

This operation can be implemented using a spatial filter of m X n in which all coefficients have value 1/mn. A mean filter smooths local variations in an image, and noise is reduced as a result of blurring.

3.2 Geometric mean filter

The given expression can be used to restore an image

$$f(x,y) = \Big[\prod_{(s,t)\in S_{xy}} g(s,t)\Big]^{\frac{1}{mn}} \quad (11)$$

The product of the pixels in the mask provides restored pixel by raising the power 1/mn. It provides more smoothing

compare than arithmetic mean filter, but loss image details in less.

3.3 Harmonic mean filter

The expression for Harmonic mean filter is

$$f(x,y) = \frac{mn}{\sum_{(s,t)\in S_{xy}} \frac{1}{g(s,t)}} \quad (12)$$

It works well for gaussian noise.

3.4 Contraharmonic mean filter

The expression for contraharmonic mean filter is

$$f(x,y) = \frac{\sum_{(s,t)\in S_{xy}} g(s,t)^{Q+1}}{\sum_{(s,t)\in S_{xy}} g(s,t)^{Q}} \quad (13)$$

where Q is order of the filter. Q might have values of 0,1 and –1.

3.5 Median filter (MF)

The best-known order-statistic filter in digital image processing is the median filter. It is a useful tool for reducing salt-and-pepper noise in an image. The median filter [2] plays a key role in image processing and vision. In median filter, the pixel value of a point p is replaced by the median of pixel value of 8-neighborhood of a point 'p'. The operation of this filter can be expressed as:

$$f(x,y) = \underset{(s,t)\in S_{xy}}{median} \{g(s,t)\} \quad (14)$$

The median filter is popular because of its demonstrated ability to reduce random impulsive noise without blurring edges as much as a comparable linear lowpass filter. However, it often fails to perform well as linear filters in providing sufficient smoothing of nonimpulsive noise components such as additive Gaussian noise [3]. One of the main disadvantages of the basic median filter is that it is location-invariant in nature, and thus also tends to alter the pixels not disturbed by noise.

3.6 Max filter

Max filters are very useful for finding the brightest points in an image.

$$f(x,y) = \underset{(s,t)\in S_{xy}}{max} \{g(s,t) \quad (15)$$

Although the median filter is by far the order-statistic filter most used in image processing, it is by no means the only one. In max filter [1] each output pixel value can be calculated by selecting maximum gray level value of N_8 (p). This filter is used for removing the pepper noise from the image. It is also proposed for Gaussian noise removal from the medical image.

3.7 Min filter

Algorithm of min filter is implemented from the following expression

$$f(x,y) = \underset{1(s,t)\in S_{xy}}{min} \{g(s,t)\} \quad (16)$$

Min filter [1] recognizes the darkest pixels gray value and retains it by performing min operation. In min filter each output pixel value can be calculated by selecting minimum gray level value of N_8 (p). It is used to remove the salt noise from the image. Salt noise has very high values in images. It is also proposed for Gaussian noise removal from the medical image.

4. RESULTS AND DISCUSSION

An attempt is made to evaluate the performance of the four linear and non-linear filters used for removing noise from the image. Experimental setup, the images are processed using the Tool Matlab. Comparisons of different filters are done by calculating the Mean Square Error (MSE) & Peak Signal to Noise Ratio (PSNR). The values are calculated by the following expression.

$$PSNR = 20 \log_{10} \frac{256}{\sqrt{MSE}} \quad (17)$$

Where MSE represents the mean square error of the estimation. For *Arithmetic mean filtering* the baby image is given as input and after filtering the performance is calculated. The MSE value is 31.2570 and the PSNR value is 66.4307 for Gaussian noise. Using *median filter* the same image is tested for performance. The MSE & PSNR values are 39.2189 & 64.4597 respectively. The best filter must give its performance high in PSNR value and low MSE value. The results obtained out of the four algorithms for different noise applications are shown in table 1.

Table 1: PSNR & MSE value

Method	PSNR value	MSE value
Arithmetic mean	66.4307	31.2570
Median	64.4597	39.2189
Max	41.5143	550.5072
Min	41.7461	536.0123

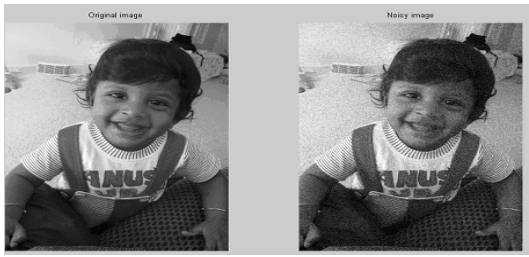

Figure 1 (a) Original image (b) Noisy image

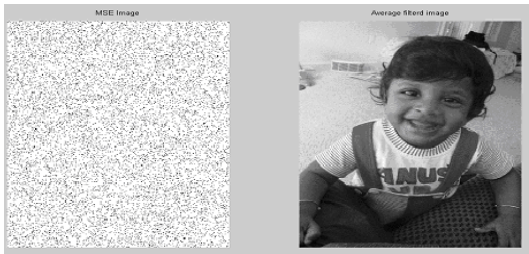

Figure 2 (a) MSE image (b) Average filtered image

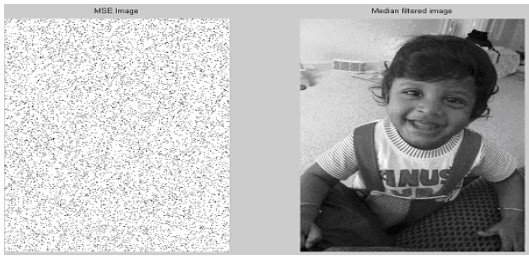

Figure 3 (a) MSE image (b) Median filtered image

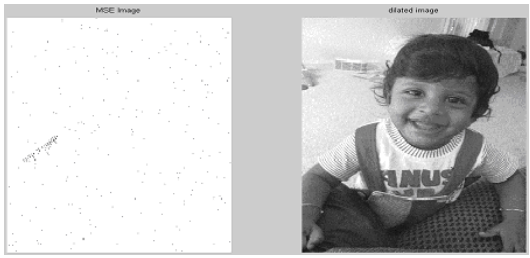

Figure 4 (a) MSE image (b) Diated image

Figure 5 (a) MSE image (b) Eroded image

5. CONCLUSIONS

In this work, we have taken various spatial filtering techniques for removal of Gaussian noise from a given image. To demonstrate the performance of the proposed techniques, the experiments have been conducted. The performance of Gaussian noise removing spatial filtering techniques is measured using quantitative performance measures such as MSE and PSNR. The experimental results indicate that the one of the filter, Arithmetic mean Filter performs significantly better than many other existing techniques and it gives the best results after successive iterations. The proposed method is simple and easy to implement.

REFERENCES:

[1] H. Hu and G. de Haan. 2006. Classification-based hybrid filters for image processing. Proc. SPIE, Visual Communications and Image Processing. 6077, 607711.1-607711.10.

[2] Hakan Güray Senel, Richard Alan Peters and Benoit Dawant. 2002. Topological Median Filter. IEEE Trans on Image Processing. 11(2): 89-104.

[3] How-Lung Eng, *Student Member*, *IEEE*, and Kai-Kuang Ma. 2001. Noise Adaptive Soft-Switching Median Filter : IEEE Transactions On Image Processing, VOL. 10, NO. 2.

[4] Ioannis Pitas, Anastasias N Venetsanopoulos. 1990. Nonlinear Digital Filters: Principles and Applications. NJ: Springer Publisher.

[5] J. W. Tukey. 1974. Nonlinear (nonsuperposable) methods for smoothing data. In: Proc. Congr. Rec. EASCOM '74. pp. 673-681.

[6] Klaus Rank and Rolf Unbehauen. 1992. An Adaptive Recursive 2-D Filter for Removal of Gaussian Noise in Images. IEEE Transactions on Image Processing: 431-436.

[7] Mamta Juneja and Rajni Mohana. 2009. An Improved Adaptive Median Filtering Method for Impulse Noise Detection. International Journal of Recent Trends in Engineering. 1(1): 274-278.

[8] P. Kuosmanen and J. Astola, "Fundamentals of Nonlinear Digital Filtering," CRC Press Inc.,Boca Raton, 1998.

[9] R. Gonzalez and R. Woods. 1992. Digital Image Processing. Adison -Wesley, New York.

[10] S. Peng and L. Lucke. 1995. A hybrid filter for image enhancement. Proc. of International Conference on Image Processing (ICIP). 1: 163-166.

[11] Yanchun Wang, Dequn Liang, Heng Ma and Yan Wang. 2006. An Algorithm for Image Denoising Based on Mixed Filter. Proceedings of the 6th World Congress on Intelligent Control and Automation. June 21-23. pp. 9690-9693.

International Journal of Science and Engineering Applications (IJSEA)
Volume 1 Issue 2, 2012, ISSN - 2319-7560 (online)

Algebraic Modeling of a field-controllable Magneto-rheological fluid damper

L.BalaMurugan
Anna University,
Chennai-600 025, India

J.Jancirani
Anna University,
Chennai-600 025, India

Abstract: In this paper a modified parametric algebraic model was proposed to capture the hysteretic behaviour of the Magneto-rheological (MR) damper. The superiority of the proposed modified model was shown by comparing it with the algebraic model. It is observed that although two models are comparable at lower voltage inputs of 1V, 2V and 3V the modified algebraic model is remarkably successful at higher voltage inputs of 5V and 7V at the highest excitation velocity of 200m/s over the algebraic model. Apart from its accuracy, modified algebraic model is also more preferable in terms of its low computational expenses compared to differential modified Bouc-Wen's model which is highly computationally demanding. Therefore it was concluded that the proposed modified algebraic model can be used to develop more effective control algorithms for such devices.
Keywords: MR damper; algebraic model; Bouc-Wen's model.

1. INTRODUCTION

For semi-active control the technologies available are based on devices with variable orifices (electrohydraulic dampers) or on devices with fluids capable of varying their viscosity as a function of electric or magnetic field (electro-rheological and magneto-rheological dampers).Recently, the semi-active suspension based on MR damper has attracted more attention [1–4] because of its fast response characteristic to magnetic fields, insensitivity to temperature fluctuations or impurities in the fluid, obtainment of convenient power and wide control bandwidth. However, the practical use of MR dampers for control is significantly hindered by its inherently hysteretic and highly nonlinear dynamics. The dislocation movement and plastic slipping among molecular chains or crystal lattices consume energy such that the restoring force of an MR damper always delays the input displacement or velocity. This phenomenon of energy dissipation is generally referred to as hysteresis. Therefore, a dynamic hysteresis model is needed to simulate the hysteresis phenomenon of MR dampers. To this end, various models have been proposed in the literature such as parametric viscoelastic-plastic model based on the Bingham model [5], the Bouc–Wen model [6], non-parametric models [7], and many more. Thus the success of MR dampers in semi-active control is determined by the accurate modelling of the MR damper.

In this paper the MR damper is modelled by the proposed modified algebraic model. Apart from its accuracy, modified algebraic model is also more preferable in terms of its low computational expenses compared to differential modified Bouc-Wen's model which is highly computationally demanding. Such a formulation is new which enhances the performance of the semi-active control. The MR damper parameters of the model used in the study correspond to an RD-1005 MR damper (made by Lord Corporation Ltd). The model parameters are determined such that the model characteristics fit very closely the experimental hysteretic behaviour of the MR damper using MATLAB curve fitting. It is obtained by minimizing the mean square error between the model and experimental results for the minimum (1V) and maximum (7V) input voltages.

2. MODELING THE HYSTERETIC BEHAVIOUR OF MR DAMPER

The MR damper used in the vehicle model with semi-active suspension is an RD-1005 MR damper (made by Lord Corporation Ltd). It is a twin tube MR damper whose schematic, the actual assembly and the components are shown in Fig. 1

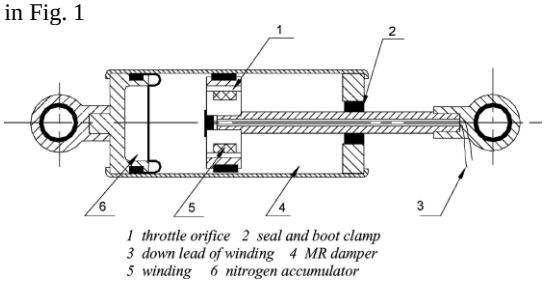

Figure-1. Structure of an RD-1005 damper [8].

As a controllable damper, it is subject to the maximal input displacement of 52 mm, the maximal voltage of 12 V. RD-1005 MR damper is tested by Guo and Hu[8] for sinusoidal excitation with a stroke length of 15mm and a fixed frequency of 2 Hz . The test has been performed for five cycles for voltages of 1.0, 2.0, 3.0, 5.0 and 7V. The measured force-velocity data for the RD-1005 MR damper is shown in Figure-2.

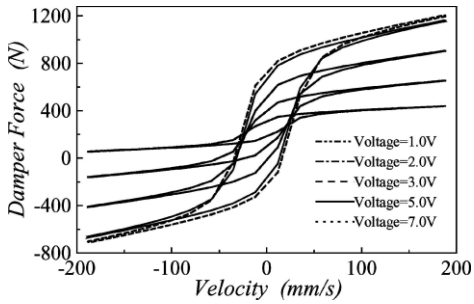

Figure-2. Force vs. velocity of RD-1005 MR damper at 2 Hz sinusoidal excitation [8].

The algebraic model proposed by Guo and Hu[8] is adopted and modified to give more accurate results. The model is given by

$$F(t) = f_0 + C_b\dot{x}(t) + \frac{2}{\pi} f_y \tan^{-1}\{k[\dot{x}(t) \quad x_0 \operatorname{sgn}(x(t))]\} \qquad (1)$$

where F represents the damping force of the MR damper, f_0 the preload of the nitrogen accumulator, C_b the coefficient of viscous damping, f_y the yielding force, k the shape coefficient, $\dot{x}_0$ the hysteretic velocity, $\dot{x}$ and $\ddot{x}$ the excitation velocity and acceleration of the piston in the damper, respectively. This mathematical model is developed based on some physical phenomena. While the first term is to represent the preload force of the pressurized nitrogen gas in the accumulator, the second term is to describe the viscous force of the damper and the third one is to reflect the observed hysteretic behaviour, respectively. The mathematical descriptions of the first two terms come from classical mechanics, whereas of the third one is developed based on the definition of a trigonometric arctangent function which best resembles the characteristic force–velocity curve of the damper. Further, the two terms in the braces of the arctangent function are to account for the lag in the force response to a sinusoidal excitation. In the model $x(t) = a\sin(\omega t), \dot{x}(t) = a\omega\cos(\omega t), x(t) \quad a \;^2\sin(\;\; t)$ where a is the displacement amplitude and ω is the angular velocity. In equation (1) f_0, C_b, f_y, k, and $\dot{x}_0$ are the unknown parameters and to be determined on the basis of experimental data by using least-square curve fitting method.

In order to validate the algebraic model, Guo and Hu[8] compared the measured damper force and the predicted damper force obtained from the algebraic model are shown in Figs. 3

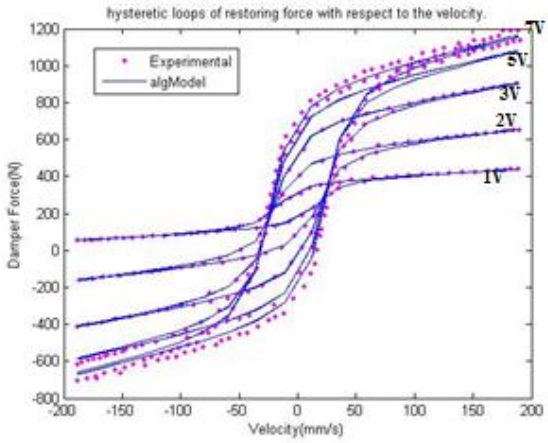

Figure-3. force vs. velocity comparisons between the algebraic model predictions and experimental data

It is observed that there is a general good agreement between the estimated and measured values except for higher voltage inputs of 5V and 7V at the highest excitation velocity of 200mm/s (see also Figure-4). The measured force-velocity data for the MR damper presented in Figure-2 suggests nonlinear dependence of the force on the applied voltage. Starting from this point, the model given in Eq. (1) is modified by multiplying an incremental nonlinear voltage function in order to improve the agreement.

$$f_d = f_0 + C_b\dot{x}(t) + \frac{2}{\pi} f_y \tan^{-1}\{k[\dot{x}(t) \quad x_0 \operatorname{sgn}(x(t))]\} *$$
$$(1 + \frac{k_2}{1 + e^{-a_2((\frac{V}{0.16}) - I_0)}} \quad \frac{k_2}{1 + e^{-a_2 I_0}}) \qquad (2)$$

The nonlinear incremental behaviour of the voltage is characterized by an asymmetric sigmoid function with a bias in the lateral axis [9]. The function must also exhibit post-yield limiting behaviour of the damping force attributed to the rheological properties of the MR fluid. The nonlinear voltage function k_2 and a_2 are positive constants and I_0 is an arbitrary constant representing the bias. The parameters are determined on the basis of experimental data by using least-square curve fitting method.

For instance, one arrives at the following mathematical model of RD-1005 MR damper for model parameter estimates, when $a \le 15mm$ and $f = \frac{\omega}{2\pi} = 2Hz$, respectively. Substituting $\dot{x}(t) = a\omega\cos(\omega t)$ into equation (1) yields

$$f_d(-a\omega^2\sin(\omega t), a\omega\cos(\omega t), V) = 247 + \frac{1.51}{1 + 10.34e^{-1.04V}} a \quad \cos(\;\; t)$$
$$+ \frac{2}{\pi}\frac{710}{1 + e^{-1.1(V-2.3)}} \tan^{-1} * \{0.0725[a\omega\cos(\omega t) \quad \frac{40}{1 \quad 1.81e^{\;0.2V}} \operatorname{sgn}(\sin \;\; t)]\}$$
$$(1 + \frac{500}{1 + e^{-(0.00001)((\frac{V}{0.16}) \;\; 0.1375)}} \quad \frac{500}{1 + e^{-(0.00001)(\cdot\; 0.1375)}}) \qquad (4)$$

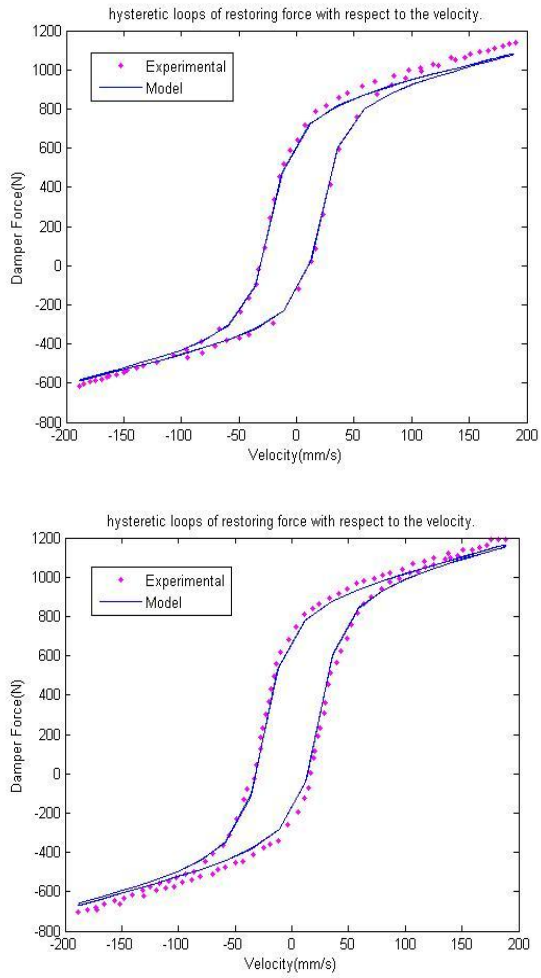

Figure-4. Hysteretic loops of damping force of RD-1005 MR damper with respect to velocity obtained from the model given by Eq.(1) at voltage inputs of 5 and 7V.

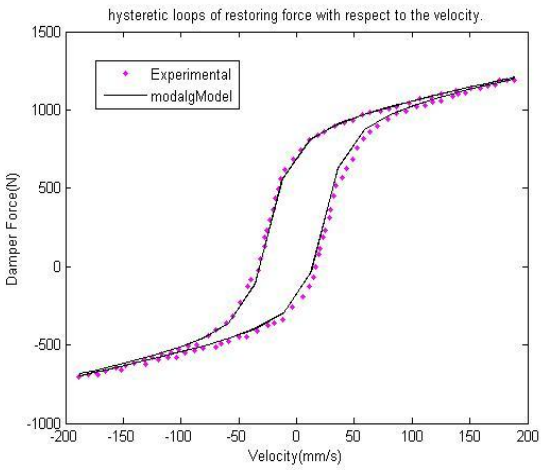

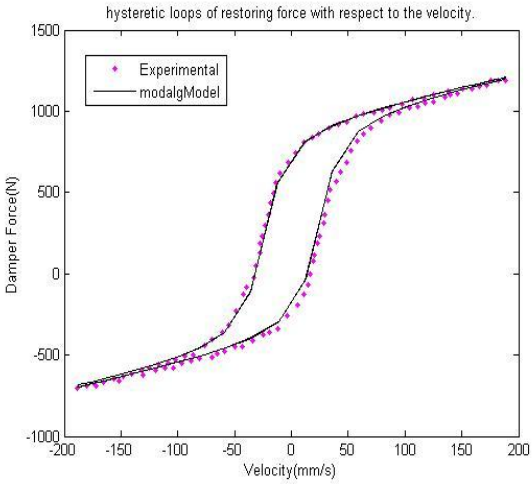

Figure-5. Hysteretic loops of damping force of RD-1005 MR damper with respect to velocity obtained from the model given by Eq.(2) at voltage inputs of 5 and 7V.

3. CONCLUSION

This paper presents a new modified algebraic model, in which algebraic model have been modified by multiplying an incremental nonlinear voltage function, was employed to describe the hysteretic behaviour of the MR damper. The unmodified and modified forms of the algebraic model, which are parametric in nature, were compared with the experimental data. It was shown that the proposed modified algebraic model removed the disagreement at the mention higher voltage input and higher velocity region. This is presumably due to effect of the multiplied incremental nonlinear voltage function to the algebraic model. Hence it was deduced that the proposed modified algebraic model could overcome the shortcomings of the original algebraic model. Apart from its accuracy, modified algebraic model is also more preferable in terms of its low computational expenses compared to differential modified Bouc-Wen's model which is highly computationally demanding. It is hoped that the present improved model will aid to develop more effective control strategies and algorithms for MR dampers.

REFERENCES

1. H.P. Du, K.Y. Sze, and J. Lam, Semi-active H-infinity control of vehicle suspension with magneto-rheological dampers, J. Sound Vibr. 283(3–5) (2005), pp. 981–996.

2. X.B. Song, M. Ahmadian, S. Southward, and L.R. Miller, An adaptive semi-active control algorithm for magneto rheological suspension systems, J. Vib. Acoust.-Trans. ASME 127(5) (2005), pp. 493–502.

3. M. Biglarbegian, W. Melek, and F. Golnaraghi, A novel neuro-fuzzy controller to enhance the performance of vehicle semi-active suspension systems, Veh. Syst. Dyn. 46(8) (2008), pp. 691–711.

4. C.M.D. Wilson and M.M. Abdullah, Structural vibration reduction using self-tuning fuzzy control of magneto rheological dampers, Bull. Earthquake Eng. 8(4) (2010), pp. 1037–1054.

5. Wereley NM, Lindler J, Rosenfeld N, Choi YT. Biviscous damping behavior in electrorheological shock absorbers. Smart Materials and Structures 2004;13: 743–52.

6. Spencer Jr. BF, Dyke SJ, Sain MK, Carlson JD. Phenomenological model of a magneto-rheological damper. Journal of Engineering Mechanics, ASCE 1997;123:230–8.

7. Song X, Ahmadian M, Southward SC. Modeling magneto-rheological dampers with multiple hysteresis nonlinearities. Journal of Intelligent Material Systems and Structures 2005;16(5):421–32.

8. Guo D, Hu H. Nonlinear-Stiffness of a magneto-rheological fluid damper. Nonlinear Dynamics 2005;40:241–9.

9. Ma X Q, Rakheja S and Su C Y 2007 Development and relative assessments of models for characterizing the current dependent hysteresis properties of magneto-rheological fluid dampers J. Intell. Mater. Syst. Struct. 18 487–502.

International Journal of Science and Engineering Applications (IJSEA)
Volume 1 Issue 2, 2012, ISSN - 2319-7560 (online)

Production of Tannase using *Aspergillus niger* by Submerged Fermentation

Mohan Kuppusamy
Department of Chemical Engineering
Annamalai University
Annamalainagar,
Tamilnadu, India

Viruthagiri Thangavelu
Department of Chemical Engineering
Annamalai University
Annamalainagar,
Tamilnadu, India

Suresh Baladhandayutham
Department of Chemical Engineering
DDE, Engineering Wing
Annamalai University
Annamalainagar,
Tamilnadu, India

Abstract: A study on optimization of submerged fermentative production of tannase by *Aspergillus niger* was carried out. *Aspergillus niger* (MTCC 3557) was used for maximum production of Tannase enzyme and the factors affecting the production were optimized. The optimum conditions for maximum tannase enzyme production in the Submerged Fermentation (SmF) using *Aspergillus niger* was obtained with an initial tannic acid concentration of 3% (w/v) at 35°C, Initial pH of 5.5 and a fermentation period of 96h.The substrates Betalnut husk and Plantain flower gave a maximum tannase production of 19.3 U/ml and 17.89 U/ml respectively.

Keywords: Submerged fermentation, Tannase, Agro residue, Aspergillus niger. optimization

1. INTRODUCTION

Tannin acyl hydrolase commonly known as tannase, catalyses the hydrolysis of ester and depside bonds in hydrolysable tannins such as tannic acid, resulting glucose and gallic acid [1]. It is extensively used in food, beverages like tea and coffee, pharmaceutical and chemical industries. The major commercial application of this enzyme is in the hydrolysis of gallotannin to Gallic acid, is an intermediate required for the synthesis of an antifolic, antibacterial drug trimethoprim[2]. Tannase is also used in the preparation of instant tea, wine, beer and coffee-flavored soft drinks and also as additive for detannification of food. Many fungi, such as Aspergillii, Penicillii, Fusaria, and Trichoderma [3–6] as well as yeast like Candida sp., and Saccharomyces cerevisiae [7] have been reported to be tannase producers. On the other hand, few bacteria are known to produce tannase and include certain species of Bacilli, Corynebacterium sp., Lactobacillus sp., and Serratia sp., [8, 9]. In Industrial level tannase is mainly produced by Aspergillus species under submerged fermentation (SmF).The SmF is widely used for enzyme production because it offers many advantages like uniform process conditions namely concentration, Temperature, pH, aeration and agitation in the bioreactors [10]. Many authors reported the tannase production by *Aspergillus* species in the medium containing pure tannic acid as both inducer and carbon source. Agro residues and forest products are generally considered as the best sources of tannin rich substrates for SmF [11].

2. MATERIALS AND METHODS

2.1 Substrate preparation

Powdered Agro residues were used for the production of Tannase enzymes. The Agro residues betalnut husk and plantain flower were powdered to 100 mesh (0.15 mm) fine powders using laboratory grinder at 3000 rpm and was preserved in a sealed plastic bag at 4°C to prevent any possible degradation or spoilage.

.

2.2 Microorganism and culture maintenance

The tannase producing fungal culture *Aspergillus niger* (MTCC 3557) was obtained from IMTECH, Chandigarh and was used for tannase production. The fungal culture was maintained on Czapek Dox media agar slants supplemented with 1 % (w/v) tannic acid as the sole carbon source. The fungal strain was subcultured periodically, grown at 30ºC for 7 days. The well grown culture was stored at 4°C in a refrigerator and used for further subculturing.

2.3 Production of Tannase in submerged fermentation (SmF)

100 ml of Czapek Dox medium in 250 ml Erlenmeyer flask was inoculated with the *Aspergillus niger* spore suspension. The composition of the Czapek Dox medium used for tannase enzyme production was Tannic Acid - 10 g/L, Sodium nitrate - 6 g/L, Potassium dihydrogen orthophosphate- 1.52 g/L, Magnesium sulphate- 0.52 g/L, Potassium chloride- 0.52 g/L, Ferrous sulphate- 0.01 g/L and Zinc sulphate- 0.01 g/L. 3 gm of substrates were added separately to the Czapek Dox medium for studying their effect on the enzyme production. The cultures were grown at 30°C, 140 rpm for six days in an incubator shaker. The samples were withdrawn at regular intervals of 24 h. The biomass was separated by the filtration through Whatman No.1 filter paper. The cell free culture broth was assayed for the tannase activity.

2.4 Tannase assay

Tannase activity was estimated by the method of Mondal and Pati [12]. 0.1 ml of enzyme solution was incubated with 0.3 ml of 1.0% (w/v) tannic acid and add 5 ml of 0.2 M acetate buffer (pH 5.0) at 40 °C for 10 min and then the enzyme production was stopped by cooling to 0°C by the addition of 2 ml Bovine Serum Albumin (BSA) (1 mg/ml), which precipitates the remaining tannic acid simultaneously A control without the enzyme was incubated and the samples were analyzed. The tubes were then centrifuged

(5,000 x g, 10 min) and the precipitate was dissolved in 2 ml of Sodium Dodecyl Sulphate (SDS) – triethanolamine (1% w/v SDS in 5% v/v triethanolamine) solution and the absorbency was measured at 550 nm after addition of 1 ml of $FeCl_3$ (0.01 M $FeCl_3$ in 0.01N HCl).
One Unit of the tannase enzyme is defined as the amount of enzyme required to hydrolyse 1µmole of ester linkage of tannic acid in 1 min at specific condition.

3. RESULTS AND DISCUSSION

3.1 Effect of substrate on production of Tannase

The effect of substrate on tannase enzyme activity in submerged fermentation using *Aspergillus niger* was studied by conducting experiments with substrates Betalnut husk and Plantain flower. The flasks containing Czapek Dox media was incubated with 3% (w/v) of the above mentioned substrates in an incubated rotary shaker at 35^0C, pH 5.5 and 200 rpm. The samples were drawn at regular time intervals of 24 h and analyzed for tannase activity at 24h, 48h, 72h, 96h, 120h and 144h. The results are given in Table 1 and Fig.1 for tannase activity obtained at different timings with substrates Betalnut husk and Plantain flower. The substrates Betalnut husk and Plantain flower gave the maximum tannase activity of 19.3 U/ml and 17.89 U/ml respectively at a fermentation period of 96 h. This higher production with Betalnut husk and Plantain flower may be due to the higher tannin content and also the substrates are easily metabolizable by *A.niger*. After 96h of fermentation, the enzyme production was found to decrease because of the inhibition and denaturation of tannase enzyme. The maximum tannase production was obtained with substrates Betalnut husk and Plantain flower and were selected for further studies on tannase enzyme production for 96h. Sabu et al reported that 96h of fermentation period gave the maximum tannase production with palm kernel cake as substrate [13] which is in good agreement with the current results obtained.

Table 1. Effect of Substrate on production of Tannase using *Aspergillus niger*

Incubation Time (h)	Tannase Activity (U/ml)	
	BETALNUT HUSK	PLANTAIN FLOWER
0	0	0
24	6.85	5.78
48	11.22	10.11
72	14.21	13.64
96	19.3	17.89
120	15.32	13.12
144	10.25	8.33

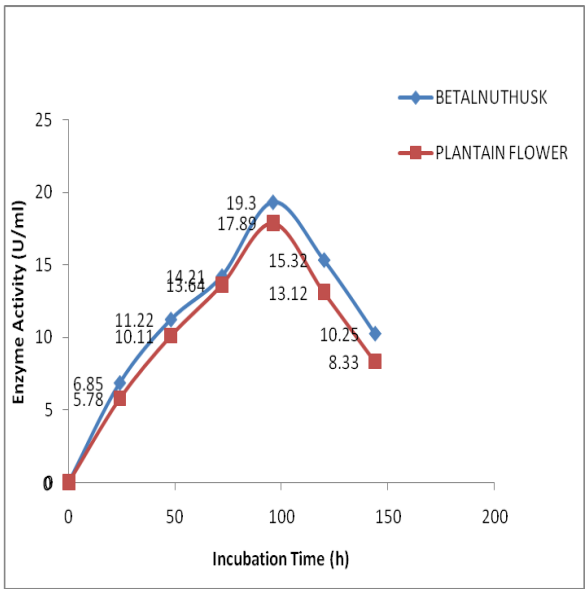

Fig 1. Effect of Substrate on production of Tannase using *Aspergillus niger*

3.2 Effect of Temperature on production of Tannase

The effect of temperature on tannase enzyme production was studied by conducting experiments at different temperatures namely 25°C, 30°C, 35°C, 40°C and 45°C keeping other parameters constant at pH 5.5, 200 rpm with the tannic acid concentration of 3%(w/v) .The results are given in Table 2 and Fig 2. As temperature was increased the maximum tannase enzyme production was found to increase rapidly. The maximum enzyme production obtained were 4.08 U/ml, 5.09 U/ml, 12.48 U/ml, 10.84 U/ml and 7.22 U/ml at 25°C, 30°C, 35°C, 40°C and 45°C respectively with Betalnut husk as a substrate. The maximum enzyme production obtained with Plantain flower as a substrate were 4.01 U/ml, 4.56 U/ml, 10.10 U/ml, 6.86 U/ml and 3.45 U/ml at 25°C, 30°C, 35°C, 40°C and 45°C respectively. At low temperatures 25°C and 30°C the rate of enzyme production was found to be less and the maximum enzyme production was found to be less. At high temperature of 40°C and 45°C the growth rate of *A.niger* was found to be less and this phenomena is similar to catalyst deactivation or catalyst poisoning in chemical catalysts. The enzyme probably got denatured which in turn resulted in less enzyme production. The maximum tannase enzyme production of 12.48 U/ml and 10.10 U/ml were obtained at 35°C and was chosen as the optimum temperature for Betalnut husk and Plantain flower as substrates respectively. The optimum temperature 35°C was used for further studies. The optimum temperature was 30°C for various fungi such as *A. tamari* [14], *A. niger*[15] and *A.flavus*[16] which is in good agreement with the current results obtained.

Table 2. Effect of Temperature on Production of Tannase using *Aspergillus niger*

Temperature (ºC)	Tannase Activity (U/ml)	
	BETALNUT HUSK	PLANTAIN FLOWER
25	4.08	4.01
30	5.09	4.56
35	12.48	10.10
40	10.84	6.86
45	7.22	3.45

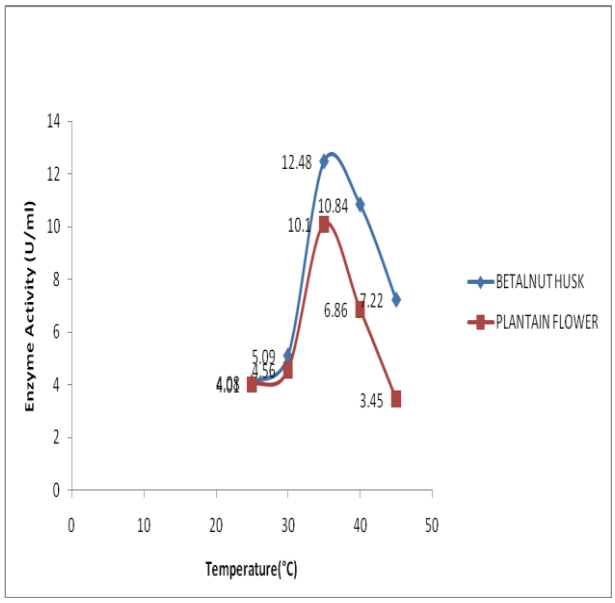

Fig 2: Effect of Temperature on the production of Tannase using *Aspergillus niger*

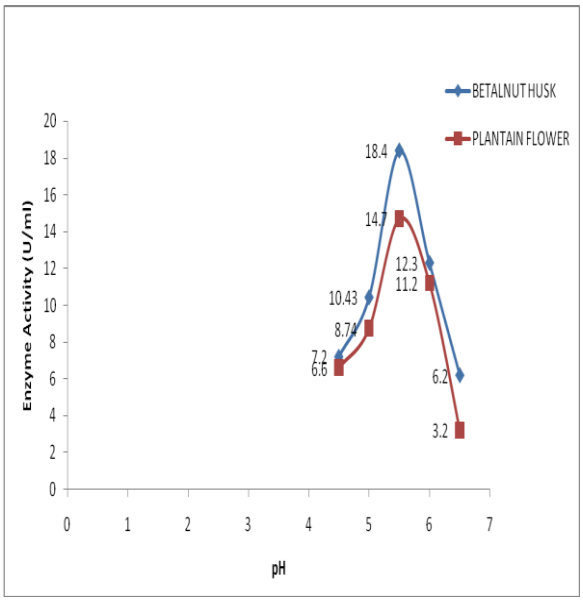

Fig 3. Effect of pH on the production of Tannase using *Aspergillus niger*

3.3 Effect of pH on production of Tannase

The effect of pH on tannase enzyme production was studied by conducting experiments at different initial pH namely 4.5, 5, 5.5, 6 and 6.5 keeping other parameters constant at temperature 35°C, 200 rpm with the tannic acid concentration of 3%(w/v).The results are given in Table 3 and Fig 3.As pH was increased the tannase enzyme production was found to increase. The growth rate was less at low pH and was maximum at pH 5.5 and thereafter the growth rate was decreasing, resulting in the lesser yield of biomass. Since the enzyme is a growth associated product, the enzyme was found to be maximum at pH 5.5.The maximum tannase enzyme production obtained were 7.2 U/ml, 10.43 U/ml, 18.4 U/ml, 12.3 U/ml and 6.2 U/ml at pH 4.5, 5, 5.5, 6 and 6.5 respectively with Betalnut husk as a substrate. The maximum enzyme production obtained with Plantain flower as a substrate were 6.6 U/ml, 8.74 U/ml, 14.7 U/ml, 11.2 U/ml and 3.2 U/ml at pH 4.5, 5, 5.5, 6 and 6.5 respectively. The maximum tannase enzyme production of 18.4 U/ml and 14.7 U/ml were obtained for pH 5.5 for Betalnut husk and Plantain flower as substrates respectively and was chosen as the optimum pH. Lekha and Lonsane [10] also reported that tannases are acidic proteins with an optimum pH 5.5. Rakeshkumar et al. [17] reported an optimum pH of 5.5 for tannase production by *Aspergillus ruber*, *Aspergillus awamori* [18] which is in good agreement with the current results Obtained

Table 3. Effect of pH on Production of Tannase using *Aspergillus niger*

pH	Tannase Activity (U/ml)	
	BETALNUT HUSK	PLANTAIN FLOWER
4.5	7.2	6.6
5.0	10.43	8.74
5.5	18.4	14.7
6.0	12.3	11.2
6.5	6.2	3.2

3.4 Effect of concentration of Tannic acid (Inducer) on production of Tannase

The effect of concentration of tannic acid on tannase enzyme production as inducer was studied by conducting experiments at different concentrations namely 1%, 2%, 3%, 4% and 5% keeping other parameters constant at temperature 35°C, pH 5.5 and 200 rpm. The results are given in Table 4 and Fig 4. As the tannic acid concentration was increased the tannase enzyme production was found to increase. The maximum enzyme production obtained were 7.44 U/ml, 12.6 U/ml, 19.1 U/ml, 17.43 U/ml and 8.32 U/ml at tannic acid concentration of 1%, 2%, 3%, 4% and 5% respectively with Betalnut husk as a substrate. The maximum enzyme production obtained were 2.86 U/ml, 7.9 U/ml, 16.1U/ml, 14.8 U/ml and 6.45 U/ml, at tannic acid concentration of 1%, 2%, 3%, 4% and 5% respectively with Plantain flower as a substrate. The maximum tannase enzyme production of 19.1 U/ml and 16.1 U/ml were obtained with Betalnut husk and Plantain flower as substrates respectively at tannic acid concentration of 3% (w/v) and was chosen as the optimum tannic acid concentration. The optimum tannic acid concentration 3% (w/v) was used for further studies. The enzyme production was found to decrease at higher inducer concentration of 4% and 5% and may be due to the substrate inhibition of inducer. At higher tannic acid concentration tannase activity was higher in SSF whereas it was repressed in submerged fermentation [19]. Actually, tannic acid at higher concentration produces complexes with protein of the organism thereby inhibits the growth and reduces the enzyme production [20].

Table 4. Effect of Tannic Acid concentration on Production of Tannase using *A.niger*

Tannic acid Concentration (%)	Tannase Activity (U/ml)	
	BETALNUT HUSK	PLANTAIN FLOWER
1	7.44	2.86
2	12.6	7.9
3	19.1	16.1
4	17.43	14.8
5	8.32	6.45

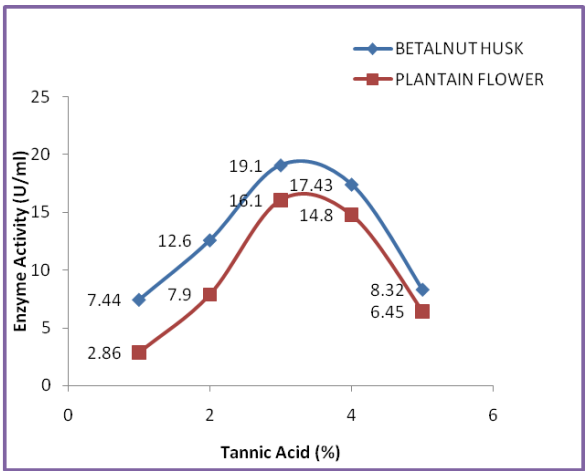

Fig 4: Effect of Tannic Acid on the production of Tannase using *Aspergillus niger*

4. CONCLUSION

The present investigation shows that agro residues such as Betalnut husk and Plantain flower were found to be the best and most cost effective substrates for the industrial production of microbial tannase. The tannase produced by *Aspergillus niger* was significant and this fact encourages further exploitation of tannase production at industrial scale. The optimum substrate concentration found to be 3 % (w/v) of Betalnut husk and Plantain flower and optimum inducer concentration of 3% (w/v) tannic acid. The optimum temperature, pH, agitation speed and fermentation period were found to be 35°C, 5.5, 200 rpm and 96h respectively.

5. ACKNOWLEDGMENTS

The authors express their sincere thanks to the Bioprocess research Laboratory, Department of Chemical Engineering, Annamalai University for providing the necessary facilities for the successful completion of this research work.

6. REFERENCES

[1] Banerjee Rintu, Mukherjee Gargi and Patra, Krushna Chandra. May 2005, Microbial transformation of tannin-rich substrate to gallic acid through co-culture method.Bioresource Technology, vol. 96, no. 8, p. 949- 953.

[2] Hadi, T.A., Banerjee, R., Bhatacharya, B.C., 1994.Optimization of tannase biosynthesis by a newly isolated Rhizopus oryzae. Bioprocess Eng. 11, 239–243.

[3] Bradoo, S., Gupta, R., and Saxena, R. K. ., 1996 Screening of extracellular tannase producing fungi. Development of a rapid and simple plate assay, J. Gen. Appl. Microbiol., 42, 325–329.

[4] Batra, A. and Saxena, R. K., 2005, Potential tannase producers from the genera Aspergillus and Penicillium, Process Biochem., 40, 1553–1557.

[5] Murugan, K., Saravanababu, S., and Arunachalam, M., 2007, Screening of tannin acyl hydrolase (E.C.3.1.1.20) producing tannery effluent fungal isolates using simple agar plate and SmF process, Bioresour. Technol., 98, 946–949.

[6] Paranthaman, R., Vidyalakshmi, R., Murugesh, S., and Singaravadivel, K, 2009, Optimization of various culture media for tannase production in submerged fermentation by Aspergillus flavus, Adv. Biol. Res., 3, 34–39.

[7] Mondal, K. C., Banerjee, D., Banerjee, R., and Pati, B, 2001, Production and characterization of tannase from Bacillus cereus KBR9, J. Gen. Appl. Microbiol., 47,263–267.

[8] Rodríguez, H., De las Rivas, B., Gómez-Cordovés, C., and Munoz, R., 2008, Degradation of tannic acid by cell-free extracts of Lactobacillus plantarum, Food Chem., 107, 664–670.

[9] Milva, P., Lucia, R. L., Roberto, A., Alessandro, E., Guido, P., Monia, R., Arianna, L., Antonio, F., Simone, G., and Silvano, E. F., 2010, Tannic acid degradation by bacterial strains Serratia spp. and Pantoea sp. isolated from olive mill waste mixtures, Int.Biodeter. Biodegr., 64, 73–80.

[10] Lekha P.K. and Lonsane B.K., 1997, Production and application of tannin acyl hydrolase. State of the art, Advances in Applied Microbiology., 44, 215–260.

[11] Lokeswari.N., 2010, Microbial production of Gallicacid by a mutant strain of *Aspergillus oryzae* using Cashew husk, Pharmacopore., 1, 112-122.

[12] K.C.Mondal, D. Banerjee, M.Jana and B.R. Pati , 2001, Colorimetric assay method for determination of tannin Acyl hydrolase (EC. 3.1.1.20) activity, *Analytical Biochemistry*, 295, 168–171.

[13] Sabu A, Pandey A, Jaafar Daud M. and Szakacs G., 2005, Tamarind seed powder and palm kernel cake: two novel agro residues for the production of tannase under solid state fermentation by *Aspergillus niger* ATCC 16620. Biores. Technol., 96, 1223-1228.

[14] Simeon Chukwuemeka Enemuor and Fredrick John Chidi Odibo, 2010, Partial purification and characterization of *Aspergillus tamari* IMI388810 (B) tannin acyl hydrolase, Archives of Applied Science Research, 2 (6): 290-299

[15] Deepanjali Lal and Joy Joseph Gardner, 2012, Production, characterization and purification of tannase from *Aspergillus niger*,European Journal of Experimental Biology, 2 (5):1430-1438

[16] Mohan Kuppusamy, Viruthagiri Thangavelu and Arunkumar Chockalingam., 2012, optimization of submerged fermentative production of Tannase by *Aspergillus flavus* International Journal of ChemTech Research, 4 (4), 1461-1467

[17] Rakesh Kumar, Jitender Sharma and Randhir Singh, 2007, Production of tannase from *Aspergillus ruber* under solid-state fermentation using jamun (*Syzygium cumini*) leaves,Microbiol research ,162, 384-390

[18] Suresh Baladhandayutham and Viruthagiri Thangavelu, 2011, Optimization and Kinetics of Solid-State Fermentative Production of Pectinase by Aspergillus awamori, International Journal of ChemTech Research, 3 (4),1758-1764.

[19] P.K.Lekha and B.K.Lonsane, 1994, Comparative Titres, Location and Properties of Tannin Acyl Hydrolase produced by *Aspergillus niger* PKL104 in Solid-state, Liquid surface and Submerged fermentations, Process Biochemistry, 29, 497-503.

[20] D.Banerjee, K.C.Mondal and B.R.Pati, 2007, Tannase production by *Aspergillus aculeatus* DBF9 through Solid state fermentation, Acta Microbiologica et Immunologica Hungarica, 54 (2):159-166.